Observations of methane net sinks in the upland Arctic tundra

Antonio Donateo[1*], Daniela Famulari[2], Donato Giovannelli[3,4,5,6,7], Arturo Mariani[8], Mauro Mazzola[9], Stefano Decesari[10], Gianluca Pappaccogli[1,11]

[1] National Research Council of Italy, Institute of Atmospheric Sciences and Climate (CNR-ISAC), 73100, Lecce - Italy
[2] National Research Council of Italy, Institute of BioEconomy (CNR-IBE), 40129, Bologna – Italy
[3] University of Naples "Federico II", Department of Biology, 80126 Napoli - Italy
[4] Institute for Marine Biological and Biotechnological Resources, National Research Council of Italy (CNR-IRBIM), Ancona, Italy
[5] Woods Hole Oceanographic Institution, Marine Chemistry and Geochemistry Department, MA, USA
[6] Tokyo Institute of Technology, Earth-Life Science Institute, ELSI, Tokyo, Japan
[7] Rutgers University, Department of Marine and Coastal Science, New Brunswick, NJ, USA
[8] GeoSystems s.r.l., 50122, Firenze - Italy
[9] National Research Council of Italy, Institute of Polar Sciences (CNR-ISP), 40129, Bologna
[10] National Research Council of Italy, Institute of Atmospheric Sciences and Climate (CNR-ISAC), 40129, Bologna
[11] JRC - ENI-CNR Aldo Pontremoli, 73100, Lecce – Italy

Correspondence to: Antonio Donateo (a.donateo@isac.cnr.it)

Abstract. This study focuses on direct measurements of CO_2 and CH_4 turbulent eddy covariance fluxes in tundra ecosystems in the Svalbard Islands over a two-year period. Our results reveal dynamic interactions between climatic conditions and ecosystem activities such as photosynthesis and microbial activity. During summer, pronounced carbon uptake fluxes indicate increased photosynthesis and microbial methane consumption, while during the freezing seasons very little exchange was recorded, signifying reduced activity. The observed net summertime methane uptake is correlated with the activation and aeration of soil microorganisms, and it declines in winter due to the presence of snow cover and because of the negative soil temperature **which triggers the freezing process of the active layer water content**, but then rebounds during the melting period. The CH_4 fluxes are not significantly correlated with soil and air temperature, but are instead associated with wind velocity, **which plays a role in the speed of soil drying. Nongrowing season emissions accounted for about 58% of the annual CH_4 budget, characterised by large pulse emissions.** The analysis of the impact of thermal anomalies on CO_2 and CH_4 exchange fluxes, underscores that high positive (> 5 °C) thermal anomalies may contribute to an increased positive flux **both in summer and winter periods, effectively reducing the net annual uptake**. These findings contribute valuable insights to our understanding of the dynamics of greenhouse gases in tundra ecosystems in the face of evolving climatic conditions. Further research is required to **constrain** the sources and sinks of greenhouse gases in dry upland tundra ecosystems, **to develop an effective reference for models in response to climate change.**

1 Introduction

The Arctic region is experiencing rapid climate change in response to the increase in greenhouse gases (GHGs), aerosols, and other climate drivers, which leads to alterations in the biogeochemical cycles of carbon and other GHGs (Stjern et al., 2019) and to the increase frequency and intensity of extreme events. This phenomenon is known as Arctic amplification (Serreze and Barry, 2011; Schmale et al., 2021). Arctic warming is essentially driven by changes in anthropogenic GHGs and short-lived climate forcers, such as methane, tropospheric ozone, and aerosols (Howarth et al., 2011; Arnold et al., 2016; Law et al., 2014; Sand et al., 2015). Methane (CH_4) and carbon dioxide (CO_2) are two of the most significant greenhouse gases that contribute to climate change, and their fluxes in the Arctic have been of great interest to researchers in recent years. Methane is a potent greenhouse gas (global average ~1.8 ppm) with a global warming potential that is about **29.8** times greater than that of carbon dioxide over a 100-year timescale (IPCC, 2023). Thus, quantifying the natural sources and sinks of CH_4 is critical for understanding and predicting how climate change will impact its cycling in northern environments. Lara et al. (2018) estimated that the Arctic tundra alone could become a net source of carbon by the mid- to late-21st century, due to the thawing of permafrost. Arctic amplification has also been found to decrease the **net uptake** of GHGs, particularly CO_2, in the Arctic region (Zona et al., 2022), because reduced soil moisture during the peak summer can limit plant productivity, thus reducing the ability of these ecosystems to capture carbon during **growing season.**

In the Arctic, methane and carbon dioxide fluxes are influenced by a variety of environmental factors, including permafrost thawing, changes in vegetation cover (especially for uptake phenomena), and in soil hydrology (Treat et al., 2015). As permafrost thaws, the organic matter it contains becomes more accessible for microbial decomposition, leading to increased methane, carbon dioxide and other greenhouse gas emissions due to microbial mediated degradation activity (Knoblauch et al., 2018). Tundra ecosystems are also known to produce methane (CH_4) as the final product of microbial metabolism through an anaerobic biotic process known as methanogenesis (Cicerone and Oremland, 1988). Methanogenesis is common in a variety of ecosystems, and it is generally found in strictly anoxic environments and in the deeper soil and sedimentary layers coupled to the final steps of the decay of organic matter (Hodson et al., 2019). **Methane uptake occurs in the atmosphere through chemical and/or photochemical oxidation, or biologically in soil and in water, through methane-oxidising bacteria and archaea (hereafter methanotrophs) that use methane as a source of energy and carbon (Serrano-Silva et al., 2014).**

Historically, most studies on methane emissions in the Arctic have focused on wetlands and wet tundra ecosystems (Tan et al., 2016), because they provide the most consistent data to evaluate total natural methane emissions in high latitudes (AMAP, 2021). The projections of future emissions in the Arctic are complicated by the multiple effects of changes in temperature and precipitation regimes in the individual ecosystems (i.e. wetlands): while a wetter, warmer climate is generally associated with an increase in natural methane emissions, drier summers can lead to increased respiration rates in soils and reduced releases

of methane. Wetland and organic carbon-rich ecosystems, however, cover a relatively small area in the Arctic region when compared with well-aerated mineral soils (Hugelius et al., 2014; Jørgensen et al., 2015; Emmerton et al., 2016). Relatively dry, well drained upland terrains and generally dry tundra ecosystems can act as significant methane sinks rather than sources over large geographical sectors of the Arctic (Emmerton et al., 2014; Jørgensen et al., 2015; D'Imperio et al., 2017; Oh et al., 2020). Due to the uncertainties in regional climate projections and in the carbon cycle response, it remains unclear whether the Arctic will play a larger role in the global CH_4 budget with future climate change (AMAP, 2021; **Treat et al., 2024**). Several studies have investigated the sources and sinks of methane in dry tundra ecosystems, especially by means of chamber measurement systems. Lindroth et al. (2022) measured the methane emissions from different types of tundra in Svalbard. The study revealed that wet tundra with waterlogged soil was a notable methane emission source, while the vegetation in the tundra served as a carbon dioxide sink. Mastepanov et al. (2008) investigated CH_4 fluxes in a dry tundra ecosystem in north-eastern Siberia, finding that the ecosystem was a small net source of CH_4, with the highest emissions occurring during the summer. This study also found that CH_4 emissions were strongly influenced by soil moisture and temperature, with wetter and warmer soils leading to higher emissions. Wagner et al. (2019), with their measurements on the southern shore of Melville Island in the Canadian Arctic Archipelago, demonstrate that net CH_4 uptake may be largely underestimated across the Arctic due to sampling bias towards wetlands. Combining in situ flux data with laboratory investigations and a machine learning approach, Voigt et al. (2023) find biotic drivers to be highly important in absorption of atmospheric CH_4 on well-drained Arctic soils. These work conclusions imply that soil drying, and enhanced nutrient supply will promote CH_4 uptake by Arctic soils, providing negative feedback to global climate change. Juncher Jørgensen et al. (2015) combining chamber in situ measurements with satellite remote sensing observations, conclude that the ice-free area of northeast Greenland acts as a net sink of atmospheric methane, and suggest that this sink will probably be enhanced under future warmer climatic conditions. Further, research on dry tundra ecosystems has focused primarily on CO_2 and CH_4 emissions during snow-free periods. However, CH_4 emissions from tundra ecosystems were not limited to the growing season. Bao et al. (2021) found that high CH_4 efflux and emission pulses can occur during shoulder seasons, such as autumn and spring thaw. This study suggests that shoulder season CH_4 emissions should be considered when assessing the total annual CH_4 emissions from tundra ecosystems. However, there is a noticeable lack of studies investigating these emissions across various seasonal phases, with a specific focus on how thermal anomaly patterns affect GHGs fluxes (Bao et al., 2021; Ishizawa et al., 2023; **Treat et al., 2024).** **Bridging the gap between the balance of CO_2 and CH_4 net flux, in dry tundra environments, with the increasing frequency and intensity of extreme events is essential for understanding the role of these ecosystems in the context of climate change.** Long-term studies covering multiple seasonal cycles have been limited owing to logistical challenges, especially during cold, snow-covered seasons (Mastepanov et al., 2008, 2013; Pirk et al., 2015, 2016; Zona et al., 2016; Taylor et al., 2018; Arndt et al., 2019; Bao et al., 2021).

This work aims to quantify the exchange fluxes of carbon dioxide and methane, between the atmosphere and the ecosystem over a long multiyear period. In particular, the objective is to understand the duration and magnitude of the exchange mechanisms and environmental drivers for CO_2 and CH_4 **for two year-rounds** (including the shoulder seasons) and their

relative importance. **This study aims to evaluate how seasonal temperature anomalies (1990-2020) affect the GHG budget. These anomalies are used as key indicators to understand how changes in temperature trends influence the overall greenhouse gas balance in the studied ecosystem.**

2 Methods

2.1 Measurement Site

Methane and carbon dioxide turbulent fluxes were measured on the "Amundsen-Nobile Climate Change Tower" (CCT) (Mazzola et al., 2016), located northwest of the village of Ny Ålesund (78°55'N, 11°56'E) in the Spitsbergen Island (Svalbard archipelago - Norway). Measurement campaign **ran from** 9th April 2021 **to** 31st March 2023, for a total of two years. The site is located on the top of a hill, and the land-cover during summer months is characterised by dry tundra or bare soil (Magnani et al., 2022). The climate is typically subarctic with a warming effect by the West Spitsbergen Ocean Current, a branch of the North Atlantic Current. The area is characterised by an average air temperature of about -10 °C in March and 6 °C in July, with about 400 mm of precipitation annually, falling mostly as snow between September and May (Lüers et al., 2014). Wind velocity average is 4.15 m s^{-1}, with a maximum monthly average of 5.47 m s^{-1} in December and a minimum in August (2.9 m s^{-1}). Wind direction is essentially from three directions, with air masses coming from south-east (42%), south-west (27%) and north/north-west (20%) (see Fig. 1a, inset). A detailed description of the meteorological and micrometeorological conditions for the measurement period was reported, respectively, in Appendix B and Appendix C. The CCT area is a semi-desert ecosystem rather than wetland or heath tundra (Uchida et al., 2009). The vegetation cover at the measurement site (Fig. A1c) was estimated to be approximately 60%, with the remainder being bare soil with a small proportion of stones (Lloyd et al., 2001, **Boike et al., 2018)**.
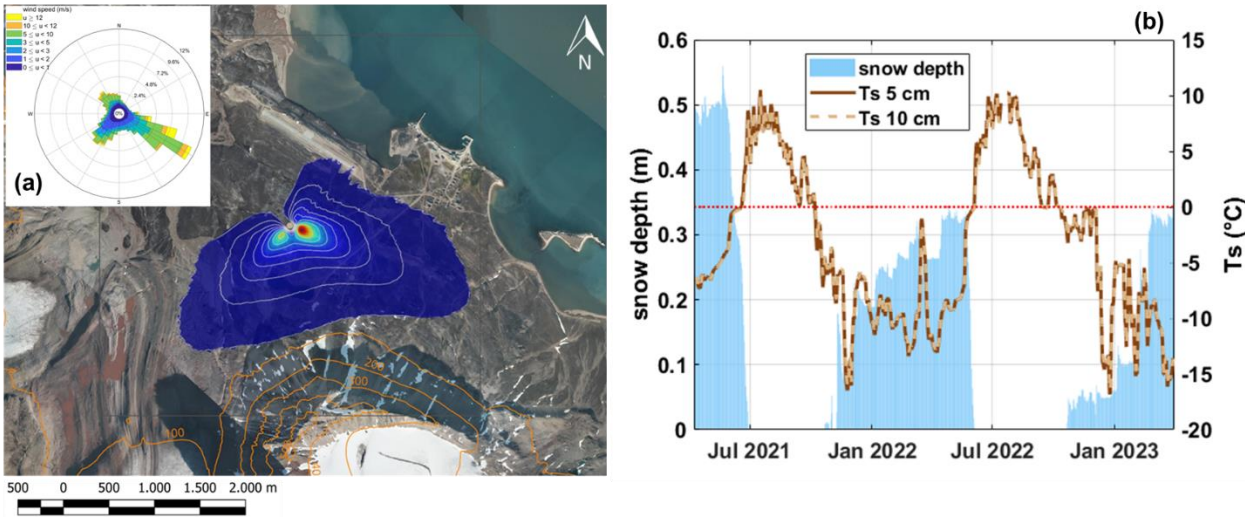
Figure 1 (a) Location map of the observation site: Ny Ålesund (Svalbard, Norway). Yellow point indicates the Amundsen-Nobile Climate Change Tower (CCT). © Norwegian Polar Institute, www.npolar.no (accessed on 12/03/2024). In the figure it was also reported foreground the flux footprint for the measurement setup (Section 2.3) at 80% contour line. In the inset the wind rose is reported for the period 2010-2023. (b) Soil temperature at two depths (5 cm and 10 cm) on the right axis and snow height (on the left axis) at the CCT site.

The vegetated portion around and within the system footprint area consists of tundra, a widespread ecosystem in Svalbard (Magnani et al., 2022). Specifically, the vegetation is dominated by low-growing vascular plants. This includes various grass and sedge species, such as *Carex* spp., *Deschampsia* spp., *Eriophorum* spp., *Festuca* spp., *Luzula* spp. Additionally, flowering plants like catchfly and saxifrage, as well as woody species like willow, are present. Notably, some locally common species like *Dryas octopetala*, *Oxyria digyna*, and *Polygonum viviparum* are also found (Fig. A1c). A moss and lichen layer are present, though the specific composition remains unclassified (Ohtsuka et al., 2006; Uchida et al., 2009; Lüers et al., 2014). In Ny Ålesund village, the thermal power plant for electricity production is the primary source of CO_2. **On the other hand,** there are few combustion engine cars on the roads and some electric vehicles **that might affect measurements occasionally.** The village lacks specific combustion sources, relying entirely on electric facilities. The airport has only two flights per week, and ship arrivals are uncommon, occurring 1-2 times a month, however, cargo handling involves heavy-duty vehicles, and it is moderately active. **All these activities are out of the measurement system footprint.**

2.2 Instruments

Standard meteorological data such as air temperature (T) and relative humidity (RH), atmospheric pressure, wind speed and direction were measured at different levels of the CCT (Fig. A1a) by means of the setup described in Mazzola et al. (2016). Snow depth at the foot at the CCT was measured with an ultrasonic range sensor (Campbell Scientific, mod. SR50A), while soil temperature (Ts) was recorded continuously using two temperature probes (Campbell Scientific, mod. 107) positioned at two different depths: 5 cm and 10 cm from the ground level. All sensors were connected to a data logger (Campbell Scientific, mod. CR-3000). Precipitation data for Ny Ålesund were downloaded from the Norwegian Centre for Climate Services web portal (https://seklima.met.no/observations/, last access on 18/03/2024). Radiation components (incoming and outgoing shortwave and longwave) were measured by means of a radiometer CNR1 (Kipp and Zonen, Netherlands) positioned at 33 m height above the ground with the sensor arm directed towards south.

To measure the eddy covariance (EC) fluxes, a three-dimensional sonic anemometer (WindMaster Pro, Gill) and two open-path gas analysers (LI-7700 for methane and LI-7500A for water vapour and carbon dioxide, both from LI-COR Biogeosciences) were used. All data were recorded at 20 Hz using a SMART Flux interface unit (LI-7550, LI-COR Biogeosciences). The instruments were mounted at a height of 15 m on the CCT above the ground level. Figure A1b shows a typical instrument mounting on the horizontal bar. Air temperature, relative humidity and pressure were also measured by the LI-COR system. The total data coverage during this experiment was 83% for the anemometer, 78% for the Li7500 and 61% for the Li7700, respectively. During this measurement period, a longer break between 8 February and 3 March 2022 was registered in the dataset due to malfunctions in the eddy covariance system. Further, the measurements suffered a break period

156   of 15 days from 5th to 20th February 2023, and stopped for 11 days in December 2022 and March 2023, respectively. Another

157   break period in the dataset must also be included in June 2022 (from the 13th to the 23rd) for a total of 10 days. These periods

158   comprise about 10% of the whole dataset.

2.3 Eddy Covariance data analysis

160   Eddy Covariance (EC) vertical turbulent fluxes of GHGs were calculated on a 30 min average using the open-source software

161   EddyPro® package (version 7.0.3; Li-COR Biosciences, USA). The micrometeorological convention of assigning positive

162   values to upward fluxes (emissions) and negative values to downward fluxes (toward the surface) was followed in this work.

163   Spikes in the 20 Hz time series were removed from the dataset and replaced by linear interpolation of neighbouring values

164   using a procedure described by Mauder et al. (2013). Data were discarded when the instrument measurement path became

165   obstructed by water (rain, dew, or snow). Data corresponding to winds blowing from a 260° - 10° sector on the back of the EC

166   setup were excluded from the analysis as they were in the wake of the tower structure (about 18% on the whole dataset). In

167   addition, the diagnostic values of the LI-7700 and LI-7500 gas analysers were used for data quality screening. For the CH_4

168   analyser, LI-7700, the relative signal strength indication (RSSI) was also considered. Methane fluxes were discarded if the

169   mean RSSI of the respective averaging interval was < 20. Spectral corrections were applied to the fluxes using the method

170   described by Fratini et al. (2012). The high and low frequency spectral attenuations were both compensated. The low-frequency

171   loss due to finite averaging time and linear detrending was corrected following Moncrieff et al. (2004). The high-frequency

172   loss due to path averaging, signal attenuation and the finite time response of the instruments was taken into account following

173   (Massmann 2000, 2001). Spectral losses due to crosswind and vertical instrument separation were corrected following Horst

174   and Lenschow (2009). Data at 30 min marked by spikes, drop-outs, discontinuities, or inputs outside absolute limits were

175   discarded from the dataset. Specifically, all data out of the 1st - 99th percentile range was discarded from the subsequent

176   analysis (about 1% of data for each variable). The processing of the raw data included an angle-of-attack correction, i.e.

177   compensation for the flow distortion induced by the anemometer frame (Nakai et al., 2006). To minimise the anemometer tilt

178   error, a three-dimensional coordinate system transformation was applied to the data set, using the planar fit method proposed

179   by Wilczak et al. (2001). This method ideally results in a null vertical wind component over a long period. The planar fit

180   coefficients are calculated for the month of May (with snow) and August (with bare tundra) in the first and second year. The

181   fit coefficients were calculated over the whole direction sector around the measurement site, spanning 60° wind sector. A linear

182   detrending procedure (Gash and Culf, 1996) was applied to the time series before the calculation of the 30 min average fluxes

183   in order to remove the effects of low-frequency variations and instrument drifts. The Webb-Pearman-Leuning (WPL)

184   correction was applied to compensate for the air density fluctuations, due to thermal expansion or water dilution, to the

185   calculation of the fluxes (Webb et al., 1980; Burba et al., 2008). Further, a correction, considered in the so-called WPL+

186   module, was applied to consider the broadening of the spectroscopic line for CH_4 due to the contemporary presence of the

187   water vapour (McDermitt et al., 2011). An important source of errors is the heat generated by the sensor body of the LI-7500

188   open-path gas analyser, which may generate convection within the sampling volume (Lafleur and Humphreys, 2007) impacting

the calculations of the CO_2 fluxes measured by the LI-7500. The correction methods proposed by Burba et al. (2008) yield unrealistic flux values **(with a large positive bias)** for this data set, especially during winter season, so that we chose not to apply this correction (Lüers et al., 2014). **Finally, a negative CO_2 flux in the cold season can result from errors propagated through the density correction, because the CO_2 density (ρ_c) can be affected by systematic biases caused by dirt contamination on the transducers and by ageing of the optical components (Fratini et al., 2014). The bias in the CO_2 flux scales linearly with the sensible heat flux H if the CO_2 density is underestimated by a constant amount, causing the CO_2 flux to be too negative (Serrano-Ortiz et al., 2008). In theory, these two fluxes (CO_2 and H) should be independent of each other in cold conditions (Tair < 0° C) when photosynthesis is suppressed (Wang et al., 2017). Thus, the correction procedure reported in Wang et al. (2017) was applied to the CO_2 flux (with a mean slope of -0.0084 μmol m^{-2} s^{-1} per W m^{-2}, R^2 = 0.92).** The detection limit (LOD) of the system was obtained using the method proposed by Finkelstein and Sims (2001). For CO_2 the LOD value resulted on average 0.3 µmol m^{-2} s^{-1}, while for CH_4 0.9 nmol m^{-2} s^{-1}. In 16% of the cases, exchange fluxes were lower than the calculated LOD, and by looking at the difference on the cumulated flux values, the contribution of these very low fluxes was of 13 g C m^{-2} (3%) for CO_2, and 0.02 g C m^{-2} (5%) for CH_4: they were excluded from the final computation, however their inclusion would not have overturned the outcome. The 30-min fluxes underwent quality control based on atmospheric stability and developed turbulence as described by Mauder and Foken (2004). This method was applied to all flux values and classified the dataset into three groups: high quality data (class 0), intermediate quality data (class 1) and low-quality data (class 2 - discarded). Following this procedure, 6% for the momentum flux, about 10% for CO_2, H_2O, CH_4 flux, and 15% for sensible heat flux H were rejected. Some quality indicators derived from the raw data statistics as described by Vickers and Mahrt (1997) were also evaluated. Fluxes related to low turbulence development conditions, i.e. not sufficient to guarantee suitable mixing, need to be identified and filtered out according to a friction velocity threshold (Aubinet et al., 2012). Such a value was computed (online tool available at https://www.bgc-jena.mpg.de/bgi/index.php/Services/REddyProcWeb - last accessed on 24/11/2023) using the bootstrapping approach described by Reichstein et al. (2005) and Papale et al. (2006). In our case, it provided u*= **0.0497** m s^{-1} and it was used to filter the CO_2 **and CH_4 fluxes dataset, discarding all data corresponding to friction velocities lower than the threshold (0.8 % of the data).**

The small gaps in the dataset, with duration less than 2 hours, were filled by a linear regression (Lüers et al., 2014). Finally, the validated data (as a percentage of the total data point) used in this work adds up to 63% (21,845 points) for H, 48% (16,649 points) for CO_2 - H_2O flux and 42% (14,555) for CH_4 fluxes, respectively. Meteorological variables were gap-filled with ERA5 data. ERA5 is a reanalysis product from the European Centre for Medium-Range Weather Forecast that provides hourly estimates for various meteorological and soil variables starting from 1959, at a spatial resolution of 25 km (https://www.ecmwf.int/en/forecasts/datasets/reanalysis-datasets/era5, last accessed on 24/03/2023). Each variable was bias-corrected using a linear fit between ERA5 and flux tower observations during periods when both were available. The CO_2 and CH_4 fluxes time series, as said previously, showed some large gaps (up to 20 days for 2022 winter), thus a gap-filling procedure has also been applied to these time series to avoid biases in the annual flux budgets. Gap filling for CO_2 fluxes was

223 implemented, firstly, through the R package REddyProc (https://r-forge.r-project.org/projects/reddyproc/; Reichstein et al.,
224 2005). This gap filling technique, based on Marginal Distribution Sampling (MDS), used as input drivers the incoming
225 shortwave radiation, air temperature, the soil temperature at 10 cm depth, relative humidity, and vapour pressure deficit.
226 **However, to take in consideration a large range of meteorological interactions and some biogeochemical variables,** a
227 random forest regression model of the fluxes was also developed (Kim et al., 2020, Knox et al., 2021) with 12 environmental
228 drivers: sensible and latent heat fluxes, air temperature, soil temperature at 10 cm depth, relative humidity, vapour pressure
229 deficit, air pressure, shortwave incoming and longwave outcoming radiation, the snow depth, the friction velocity and, finally,
230 the boundary layer height. Furthermore, the CO_2 flux (gap filled) was itself added as a driver for gap filling the CH_4 flux data.
231 Only the gaps in the flux time series were filled with the resulting flux estimates from the random forest regression model. The
232 implementation of the random forest model was developed with open-source python libraries such as Scikit-learn (Pedregosa
233 et al., 2011). After a process of model tuning the optimal values for various training parameters were found, such as the number
234 of estimators (decision trees) and the maximum depth of the model. Training of the model and model performance estimation
235 were conducted following common methodologies as reported in Dyukarev (2023), which resulted in a validation error
236 (Normalised Root Mean Squared Error) of 7.75% for CO_2 and 9.37% for CH_4 inference.
237 The ratio between wind velocity and the friction velocity in neutral atmosphere ($-0.05 < z/L < 0.005$, where z is the
238 measurement height and L is the Obukhov length) was used to evaluate the average roughness length z_0, for the site analysed
239 using a parameterisation based on similarity theory (Stull, 1988). The results gave $z_0 = 0.005 \pm 0.001$ m, with similar results
240 reported also by (Mazzola et al., 2021; Donateo et al., 2023 in the same site). Separating the winter period (with snow coverage)
241 from the summer period (without snow), z_0 values were calculated as $z_0 = 0.002 \pm 0.001$ m (winter) and $z_0 = 0.004 \pm 0.001$ m
242 (summer), respectively. A null displacement height *d* was considered for this site as obstacles of significant height are not
243 present around the site and in its footprint. Source area for scalar fluxes have been evaluated using a Lagrangian footprint
244 model proposed by Kljun et al. (2015). The results of flux footprint analysis are shown in Fig. 1 with the different influence
245 levels of the zones on the measurements. The gas fluxes measured represented a surface area of about 2.4 km^2 (considering
246 the 80% contour line) with a maximum distance of 1300 m and 1600 m in south-west and south-east direction, respectively. It
247 is worth remembering that the data in the wake of the tower structure at north-west and north-east were excluded from the
248 analysis. The flux peak contribution was in the wind direction sectors at about 130 m ($\pm$ 5 m) at south-east and south-west
249 (Fig. 1). However, the source land area was very similar for the considered wind direction sectors around the measurement
250 site, with 100% of snow coverage for the winter period. During the summer period the footprint area was over tundra coverage,
251 with about 2.4% covered by water surfaces (two arctic lakes) (Fig. 1).
252
253 **2.4 Seasonality**
254 In this work the calendar year was divided into a snow-cover season (winter), a snow-free season (summer), and a
255 thawing/freezing period, in late spring and autumn, respectively. Thawing period represents a transitional phase during which
256 the snow cover melts. Daily soil temperature and snow depth were used to define the different seasons. The start of the snow-

cover season was defined as the start of the freeze-up, i.e. the first day on which daily mean Ts at 5 cm depth is below -0.75 °C for 3 consecutive days (Oechel et al., 2014; Taylor et al., 2018; Arndt et al., 2019; Bao et al., 2021) and at the same time daily snow depth is greater than 1 cm. The end of the snow-cover season was defined as the start of thaw, i.e. the first date on which daily mean T_s at 5 cm depth rose above 0.75 °C for at least 3 consecutive days. Winter season was between the end of the freezing period (being the total solar radiation < 10 W m^{-2}) and the beginning of the thawing period. At the same time the summer season was defined as the period between the end of thawing (being the snow depth lower than 1 cm) and the beginning of the freezing period. Thawing and freezing periods are also called in the manuscript "shoulder seasons" as reported by Bao et al., 2021. Further, the winter season was divided into a first period (dark winter) in absence of solar radiation (total radiation < 10 W m^{-2}) and a second one (light winter) with an increasing total radiation greater than 10 W m^{-2}. Thereby two complete light winter (snow-covered) seasons during the study period could be defined: from 1st March 2022 to 19 May 2022 (80 days) and from 5 to 31st March 2023 (27 days). Furthermore, an initial period from 9 April 2021 to 27 May 2021 (48 days) has also been included as a snow-cover period. Two dark winter periods (snow-covered), as specified earlier without solar radiation, have been identified: from 23 October 2021 to 28 February 2022 (128 days) and from 23 October 2022 to 4 March 2023 (132 days). Two complete summer seasons were also included in the dataset: from 29 June 2021 to 07 October 2021 (100 days) and from 4 June 2022 to 13 October 2022 (131 days). Finally, two thawing and freezing periods in 2021 and 2022 were covered in this work. Specifically thawing in the month of May/June and freezing in the month of October for a total of 45 days in thawing and 22 days in freezing period.

3 Results and Discussion

3.1 CO₂ and CH₄ mixing ratio and surface fluxes

Median CO_2 mixing ratio over the whole measurement period was 413.66 ppm (average 412.30 ppm) with an interquartile range (IRQ 25th – 75th percentile) from 406.17 to 417.72 ppm (Fig. 2a). The CO_2 mixing ratio was greater during the winter period with a median value of 418.46 ppm decreasing towards the summer season, when it measured a median of 403.81 ppm with a minimum value of 396.61 ppm (Fig. 2b). The shoulder season was characterised by intermediate CO_2 concentration: the thawing season showed a median mixing ratio of 415.14 ppm greater than the CO_2 concentration in the freezing season (405.62 ppm) (Fig. 2b). The median CH_4 mixing ratio for the measurement period was 2.05 ppm (IRQ 2.04 - 2.07 ppm) (Fig. 2c). In this case, the greatest concentration was found during the dark winter season (2.06 ppm) with a decreasing trend going towards the summer season down to a median value of 2.05 ppm. The thawing and freezing seasons presented very similar values in CH_4 concentration; 2.044 and 2.043 ppm, respectively (Fig. 2d).

287

288
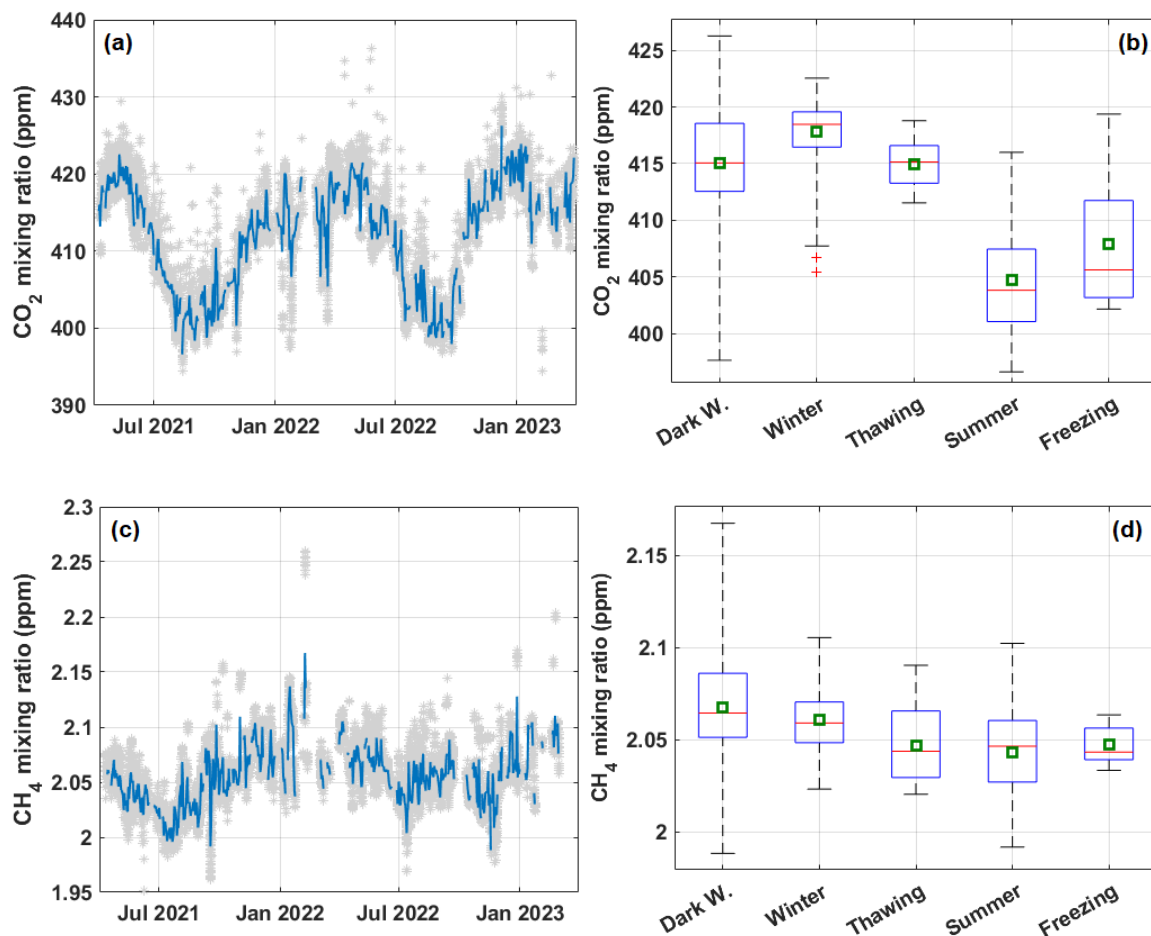
Figure 2 Time series on a daily basis (left) and whiskers-box plots (right) of (a,b) CO_2 and (c,d) CH_4 mixing ratio. In the left panels, in light grey the time series for CO_2 and CH_4 mixing ratio at 30 min resolution. In the right panels, whiskers represent max and min values, the box limits are the 25th and 75th percentiles. The red line represents the median value on a 30 min basis.

In Fig. 3a,c, the annual cycle of CO_2 and CH_4 turbulent fluxes was observed, with CO_2 and CH_4 fluxes exhibiting negative intensity for the greater part of the year. **The** CO_2 flux had a median value for the whole period of -0.032 μmol m^{-2} s^{-1} (detailed statistics in Table 1). At the same time, the median value for the CH_4 flux was -0.39 nmol m^{-2} s^{-1} (Table 1). Negative values are particularly important in CO_2 and CH_4 fluxes during the summer season (growing season) indicating a sink behaviour for the CCT site.

Table 1 Statistical analysis for the CO_2 and CH_4 fluxes in the measurement site separated into five different seasons defined in this work.

CO_2 flux (μmol m^{-2} s^{-1})

	Dark W.	Light W.	Thawing	Summer	Freezing
mean	**0.007**	**-0.157**	**-0.346**	-0.458	**-0.026**
median	**0.020**	**-0.839**	**-0.178**	-0.368	**-0.794**
25th percentile	**-0.127**	**-0.311**	**-0.500**	-0.776	**-0.140**
75th percentile	**0.155**	**-0.067**	**-0.080**	-0.133	**0.058**
min	**-0.724**	**-3.044**	**-1.519**	-1.951	**-0.236**
max	**0.966**	**0.638**	**0.106**	0.515	**0.323**

	CH_4 flux (nmol m^{-2} s^{-1})				
mean	-0.368	-0.665	-0.972	-1.375	-0.498
median	-0.175	-0.359	-0.83	-1.284	-0.688
25th percentile	-0.958	-1.018	-1.512	-2.292	-1.424
75th percentile	0.302	0.043	-0.055	-0.467	0.137
min	-4.599	-7.271	-5.594	-5.319	-3.202
max	6.993	1.779	1.207	2.673	1.842

Seasonal analysis revealed negative median values for the fluxes of CO_2, peaking in summer with -0.37 µmol m^{-2} s^{-1}. **The CO_2 fluxes showed a slightly positive median value during the dark winter (0.02 µmol m^{-2} s^{-1}), actually, due to respiration phenomena from the snow covered surface due to microbial respiration (Hicks Pries et al., 2013). At a finer time scale (30 min resolution), the CO_2 flux trend indicated the presence of positive fluxes (emissions) (Fig. 3a),** especially during the dark/light winter and the freezing period (Table 1). **As snowmelt begins, accumulated carbon dioxide may be released and exposed patches of ground with a lower albedo begin to warm, further enhancing respiration rates and CO_2. Further, during thawing season, incoming radiation reaches levels adequate for photosynthesis: the combination of increasing light, along with increases in soil temperatures can result in early photosynthesis. At the CCT site, the CO_2 flux decreased starting from the light winter (-0.84 µmol m^{-2} s^{-1}) and it continues during the thawing season (-0.18 µmol m^{-2} s^{-1}). During the fall, soil temperatures were still adequate for substantial microbial respiration. When the senescence of vascular plants advanced, respiration became the dominant process affecting carbon exchange. In addition, as soils freeze, CO_2 may be forced out of the soil towards the atmosphere. However, in the freezing period, at the CCT site, a median negative CO_2 flux has been measured (-0.79 µmol m^{-2} s^{-1}).**

A similar trend is reported for methane: during the dark and light winter periods, methane fluxes are negative, with a median value of -0.17 and -0.36 nmol m^{-2} s-1, respectively (Fig. 3d). **Treat et al. (2018) investigated methane dynamics across Arctic sites and reported negative methane fluxes during winter, attributed to cold temperatures, which inhibit methanogenesis while promoting methane oxidation in dry tundra soils. However, they also highlight methane uptake in dry tundra during colder periods. Zona et al. (2016) reported that methane emissions during the cold season**

(September to May) account for ≥50% of the annual CH₄ flux, with the highest emissions from upland tundra. In this study (Table 1), evidence of significant emission events during winter temperature fluctuations can be observed at the site. In contrast, these events diminished in the shoulder seasons, where notable **net uptake** events dominated, with -0.83 nmol m^{-2} s^{-1} during thawing and -0.69 nmol m^{-2} s^{-1} during freezing period. **Seasonal analysis revealed negative median CH₄ fluxes, peaking in summer at-1.28 nmol m^{-2} s^{-1}. Juncher Jørgensen et al. (2015) field measurements, within the Zackenberg Valley in northeast Greenland over a full growing season, showed methane uptake with a seasonal average of -2.3 nmol CH₄ m^{-2} s^{-1} in dry tundra. Wagner et al. (2019) measured a negative peak during the growing season (2009) of -4.41 ng C-CH₄ m^{-2} s^{-1} in a polar desert area at the Cape Bounty Arctic Watershed Observatory (CBAWO - Melville Island, Canada).**
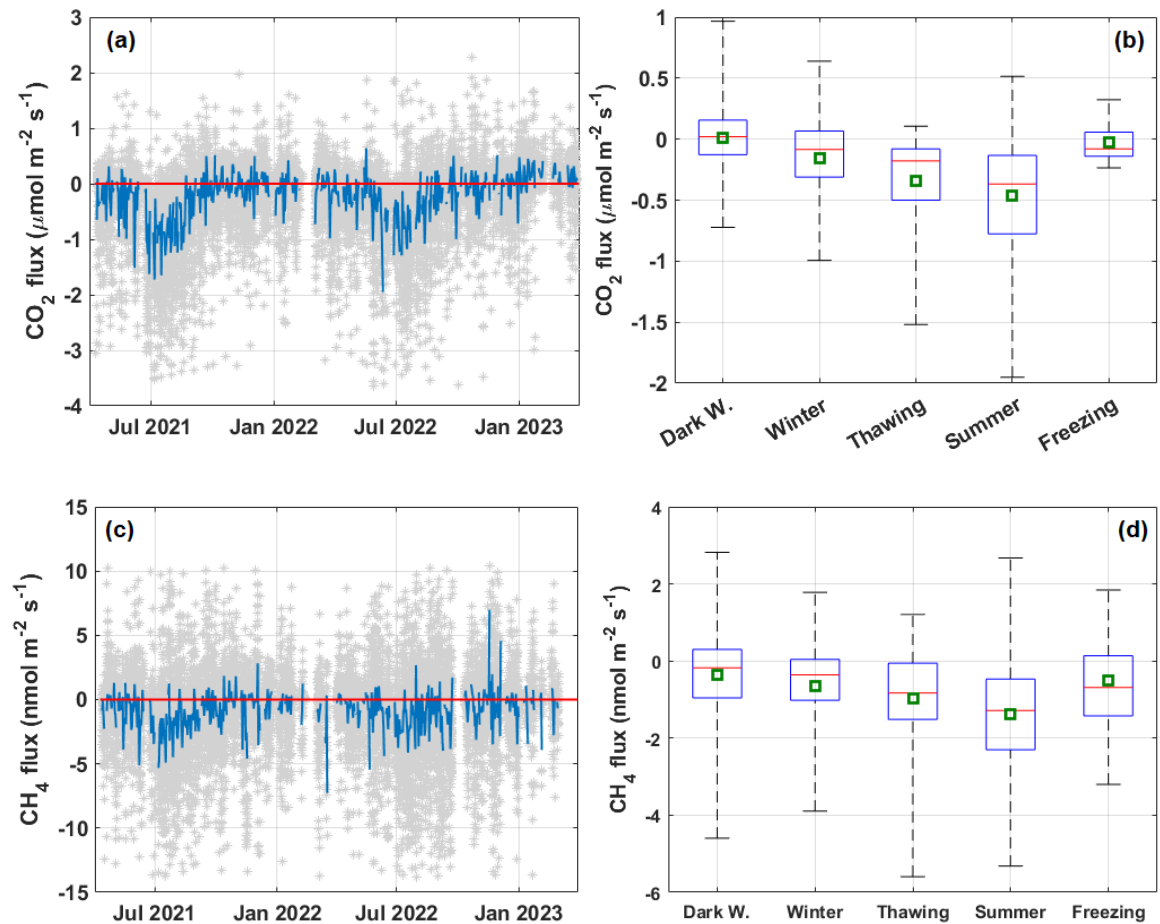
Figure 3 Time series on a daily basis (left) and whiskers-box plots (right) of turbulent vertical flux (a,b) CO₂ and (c,d) CH₄ measured at CCT. In the left panels, in light grey the time series for CO₂ and CH₄ mole fraction at 30 min resolution and the red line represent **the zero level for fluxes.** In the right panels, whiskers represent max and min values, the box limits are the 25th and 75th percentiles. The red line represents the median value and the green square the average value.

Even though a similarity between the CO_2 and CH_4 flux patterns can be observed from the time series, the exchange processes are probably led by different physical drivers. Significantly negative fluxes of CO_2 are driven by photosynthesis, while CH_4 uptake fluxes increase coinciding with a positive peak in ground temperatures **(Mastepanov et al., 2013; Howard et al., 2020). While prior research demonstrated the influence of soil temperature on methanotrophic activity (Reay et al., 2007), CH_4 fluxes at CCT site showed limited response to soil temperature, as reported later.**

3.2 CO_2 and CH_4 mass budget

The cumulative mass budgets over the two monitoring years at the CCT site ecosystem are shown in Fig. 4. Based on the budget for the whole measurement period, the study area acts as a net sink for both CO_2 and CH_4. During the study period, a CO_2 balance of almost **-257 CO_2** g m^{-2} is found, while the contribution of CH_4 uptake was estimated at approximately -0.36 g CH_4 m^{-2} **(Fig. 4, dashed red line)**. Actually, for the evaluation of the cumulated carbon, the gap filled time series should be considered (both with MDS and RF methodology, see Section 2.3). In this perspective, the total cumulative CO_2 budget over the measurement campaign was **-472** g CO_2 m^{-2} with MDS and **-650** g CO_2 m^{-2} using the RF procedure, respectively (Fig. 4a). On the other hand, CH_4 cumulative budget was about -0.76 g CH_4 m^{-2} with the RF gap filling procedure (Fig. 4b). The mean annual cumulative CO_2 budget was **-131** g CO_2 m^{-2} with MDS and **-164** g CO_2 m^{-2} with RF. **Oechel et al. (2014) reported a net CO_2 uptake during the summer season of -24.3 g C m^{-2}, while the** no growing seasons **released 37.9 g C m^{-2}, showing that these periods comprise a significant source of carbon to the atmosphere. In Treat et al. (2024) is reported for 2002–2014, a smaller CO_2 sink in Alaska, Canadian tundra, and Siberian tundra (medians: -5 to -9 g C m^{-2} year-1). Euskirchen et al. (2012) established eddy covariance flux towers in an Alaska heath tundra ecosystem to collect CO_2 flux data continuously for over three years. They measured a peak CO_2 uptake, during July, with an accumulation of -51 -95 g C m^{-2} during June–August. On average, the mean annual cumulative budget for CH_4 was -0.18 g CH_4 m^{-2} year^{-1}, calculated using gap-filled data (Table 2). This outcome lies within the same order of magnitude estimated by Dutaur et al. (2007) at the global level, reporting a net CH_4 uptake for the non-forested arctic environments (defined as "boreal other") of -0.14 g CH_4 m^{-2} year-1. Treat et al. (2018) found that tundra upland varies from CH_4 sink to source with a median annual value of 0.0 ± 0.20 g C m^{-2} year^{-1}. Lau et al. (2015) found that the CH_4 uptake rate was in the range between −0.1 to −0.8 mg CH_4-C m^{-2} day^{-1} at AHI site (Nunavut, Canada). In this work it was suggested that mineral cryosols act as a constant active atmospheric CH_4 sink (Emmerton et al., 2014) in part because of their low soil organic carbon availability, low vegetation cover and low moisture content.**

The annual budget can be further split into the five seasons considered in this study. Specifically, the CCT area acted as a CO_2 sink during the thawing and summer period with an average value of **-0.79** and -1.1 g CO_2 m^{-2} day^{-1}, respectively. **During the freezing period the quantity of absorbed CO_2 per day decreased down to almost null value (-0.01 g CO_2 m^{-2} day^{-1}), and slightly increased to a positive value during the dark winter period (0.04 g CO_2 m^{-2} day^{-1}). With the increasing amount of the solar radiation, the mass cumulative CO_2 per day decreased again (-0.25 g CO_2 m^{-2} day^{-1} for light winter). Ueyama et al. (2014) analysed seasonal CO_2 budgets across several tundra ecosystems in Alaska, reporting peak CO_2 uptake**

370 **during summer with an average value of -46 g C m⁻² due to maximum photosynthesis rates.** The same pattern was
371 followed by the CH_4 absorbed carbon mass: in this case during the thawing period was observed a value on average of -0.55
372 mg CH_4 m⁻² day⁻¹, peaking its negative maximum during the summer period (-1.29 mg CH_4 m⁻² day⁻¹). Also, in this case the
373 absorbed carbon mass decreased in the freezing period down to -0.63 mg CH_4 m⁻² day⁻¹. It was reduced to very low values
374 during the winter season with -0.26 mg CH_4 m⁻² day⁻¹ in dark winter and -0.40 mg CH_4 m⁻² day⁻¹ in light winter. **Nongrowing**
375 **season emissions accounted for 58% of the annual CH_4 budget, characterised by large pulse emissions.**
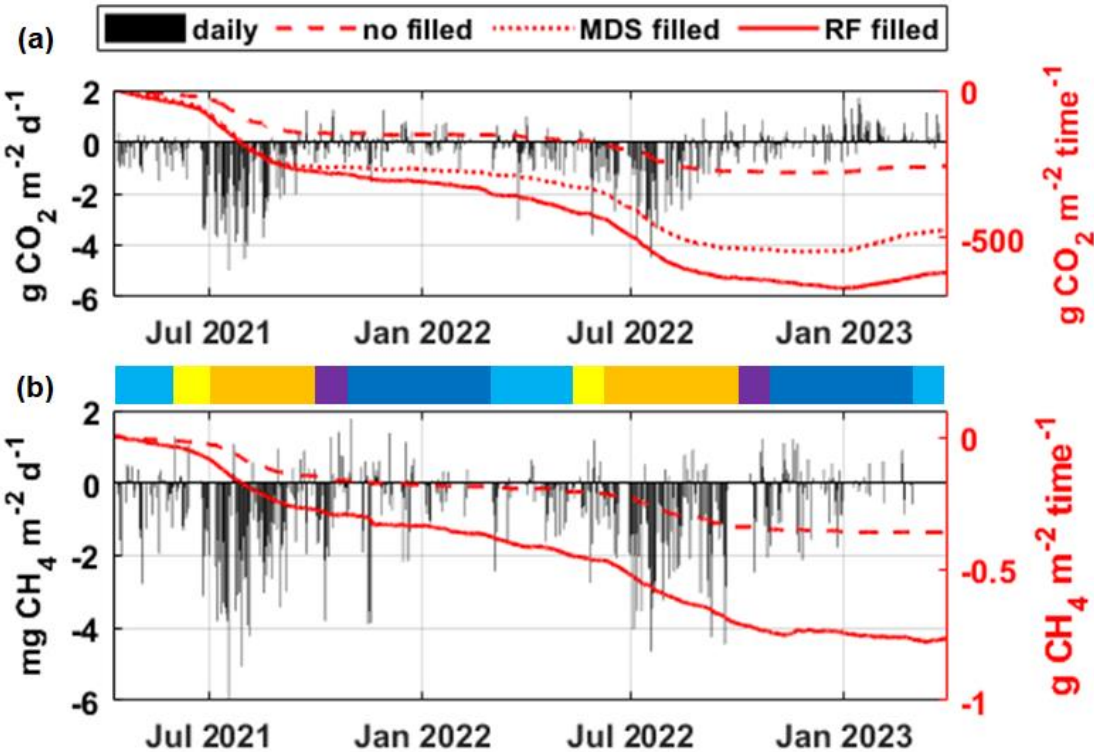
376
377 **Figure 4** Daily (black bars - left axis) and **mass** cumulative (red - right axis) ecosystem exchange for (a) CO_2 and (b) CH_4 measured at CCT
378 site. **Mass cumulative exchange for CO_2 and CH_4 was reported: dashed line for no gap filled time series, dotted line for MDS and**
379 **continuous line for RF.** Central multicoloured bar separates the time series into five different seasons: blue for light winter, yellow for
380 thawing, orange for summer, purple for freezing and navy for dark winter.
381

382 **Table 2** Mean mass cumulative g CO_2 and mg CH_4 for each season defined in this work and the mean cumulated g CO_2 and
383 mg CH_4 yearly in the measurement site. The values are reported for the original gap time series (RAW), the gap-filled dataset
384 with MDS and RF procedure.
385

CO₂ cumulated (g CO₂ m⁻²)					
Dark W.	**Light W.**	**Thawing**	**Summer**	**Freezing**	**Year**

RAW	-1.27	-7.19	-4.87	-65.97	-0.43	-65.01
MDS	-0.38	-14.25	-18.69	-126.38	-0.66	-131.37
RF	-8.04	-14.49	-19.58	-157.41	-1.04	-164.55
CH_4 cumulated (mg CH_4 m^{-2})						
RAW	-13.78	-7.47	-3.99	-73.69	-7.15	-77.52
RF	-21.35	-28.32	-29.81	-135.74	-9.88	-182.78

3.3 Physical drivers on GHGs surface fluxes

High temporal resolution measurements of CO_2 and CH_4 facilitate looking at the underlying causes of emissions, looking, for example, at the relationship between meteorological/flux variables and CH_4 fluxes (Taylor et al., 2018). Further, the importance of soil net CH_4 uptake is poorly constrained, but it is widely recognised that soil temperature, soil moisture, and substrate availability (CH_4 and O_2) are the main drivers of the temporal variations of observed and predicted net CH_4 fluxes (D'Imperio et al., 2024). Juncher Jørgensen et al. (2024) incubation studies revealed that subsurface CH_4 oxidation is the main driver of net surface-atmosphere exchange, and it responds clearly to changes to soil moisture in these dry upland environments. The production, consumption, and transport processes of CH_4 are primarily related to hydrology, vegetation, and microbial activities (Vaughn et al., 2016; Wang et al., 2022). In this work any soil hydrology measurements were available for understanding these processes, however the measured wind velocity and soil temperature have been used as proxies for soil moisture and water table depth. Previous works have shown that advection, forced by wind pumping related to atmospheric turbulence, can increase turbulent fluxes from/to the snowpack (Sievers et al., 2015). Typically, the wind pumping effect led to increased emissions flux in CO_2 resulting from ebullition and/or ventilation. This correlation was analysed for the snow-covered periods (dark/light winter) in our measurement site (Fig.5a). The scatter plot in Fig. 5a shows a quadratic relationship (the equation of the fit is reported in the figure, $R^2=0.91$) between wind speed and vertical turbulent CO_2 flux, with a clear increasing trend indicating positive fluxes for wind speed above 3 m s^{-1}. From a similar analysis, but in this case for the whole measurement period, for the CH_4 fluxes (Fig.5b), it can be observed, in this case too, a quadratic relationship with the wind velocity ($R^2 = 0.98$). In the range of low wind velocity CH_4 exchange balance is on median values very close to zero but going to greater wind speed (>10 m s^{-1}) the negative CH_4 flux (uptake) increases.
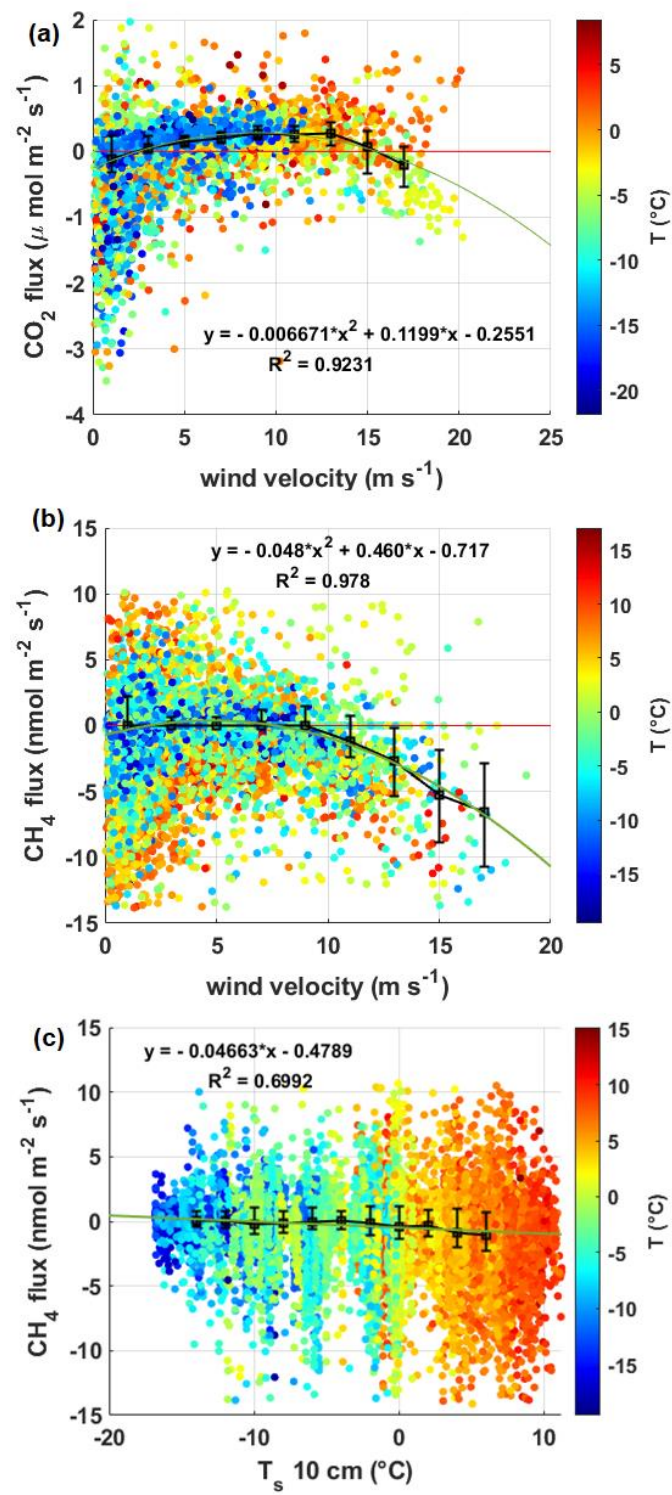
Figure 5 Scatter plot of turbulent vertical (a) CO_2 and (b) flux against wind speed. **In (a) data was selected for the snow covered period (dark and light winter). (c) Scatter plot of the vertical CH_4 flux as a function of the soil temperature Ts. Data in the panels is colour-coded according to air temperature T.**

At the CCT site, where uptake seems to outweigh emission within the flux footprint, the soil layer would be relatively depleted in methane compared to the atmospheric boundary layer. The coarse soils at CCT may therefore experience increased aeration, which could in turn aid in the transportation of CH_4-rich air from the overlying atmosphere to the methanotrophs, and/or enhance the movement of CH_4-depleted air from the soil into the atmosphere. In addition, increased aeration would provide oxygen to the deeper soil layers during the dry season, stimulating the activity of aerobic methanotrophs. Analysis through a scatter plot (Fig. 5c) depicting CH_4 flux alongside both soil and air temperature revealed a minimal correlation, indicating that variations in temperature had minimal impact on CH_4 fluxes. The extent to which temperature fluctuations affect CH_4 fluxes in the soil is heavily contingent on the depth of the microbial community responsible for these fluxes. Despite previous findings indicating that methanotroph habitats are typically situated near the soil surface at depths ranging from 3 to 15 cm (Curry, 2007; Yun et al., 2023), there was no assessment of the vertical distribution of microbial populations in the soil at the CCT site. **Overall, the observed correlation in the ecosystem uptake of methane with wind velocity suggests that the methanotrophic communities in the Svalbard soils might be stimulated by soil aeration, strongly related to its drying out during the summer. Since the CCT is also a semi-desert surface, the CH_4 uptake regulation is most directly related to the porosity and soil hydrology (not measured in this study), indirectly affected by the wind that can dry the soil and increase diffusivity for atmospheric oxygen.**

3.4 GHGs fluxes response to seasonal temperature anomalies

In this work the seasonal temperature anomalies were evaluated as possible drivers for the modifications in GHG exchange turbulent fluxes on a daily basis. This approach allowed for a comprehensive understanding of the relationship between thermal variations and corresponding flux dynamics over the considered time period. **In this study, the temperature anomalies were calculated with respect to the day of the year average values taking the period 1991-2020 as a baseline.** Figure 6 depicts the dependence of the CO_2 and CH_4 turbulent fluxes on the temperature anomalies, on a daily basis, based on a 5-day running window. **As can be observed, net uptake fluxes for both gases are most noticeable in conditions of above-zero ground temperatures, clearly indicating the summer period, but with thermal anomalies below 5°C (Fig.6c,d). The magnitude of uptake gases flux decreases with increasing positive thermal anomalies during the summer (0.04 µmol m^{-2} s^{-1} °C for the CO_2 and 0.07 nmol m^{-2} s^{-1} °C for the CH_4) until it reverses to a positive (emissive) flux, with an attenuated net uptake, for marked positive anomalies above 8°C (Fig 6a,b). This behaviour suggests that the trend is toward a null annual net uptake of CO_2, considering the increasing frequency and intensity of positive temperature anomalies. During the winter season, dark and light winter together, the gas fluxes did not show a particular trend against the thermal anomalies, with an average rate of about 0.006 µmol m^{-2} s^{-1} °C - for the CO_2 and 0.008 nmol m^{-2} s^{-1} °C for the CH_4 (Fig. 6a,b). Shoulder seasons show a positive trend between fluxes and thermal anomalies, albeit based on a tight**

442   **range of thermal anomalies. Specifically, during the freezing season, uptake and emission fluxes occur with negative**

443   **and positive anomalies, respectively (not shown here), with no a specific trend. Figure 6e,f shows the same type of**

444   **analysis for CO_2 and CH_4 fluxes during the thawing season, which presents a consistent uptake for both positive**

445   **temperature anomalies (below 10°C) and also for negative anomalies (above -5 °C). In a context of climate change,**

446   **large positive anomalies could lead to positive (or at least null) fluxes in all seasons,** while optimal situations could occur

447   during the summer, considering a lower temperature increase in this season (Bintanja and Linden, 2013**). Overall, the results**

448   **suggest a transition of CO_2 and CH_4 flux regimes to an emissive scenario (reduced net uptake) for thermal anomalies**

449   **above 10°C for all the periods considered, especially for the winter, where the thermal anomalies have a greater relative**

450   **magnitude.** The findings in this study align with the observed decrease in the net carbon reservoir in northern ecosystems as

451   air temperature rises (Cahoon et al., 2012; Zona et al., 2022). **This suggests that future increases in temperature will weaken**

452   **the ecosystem CO_2 sink strength or even turn it into a CO_2 source, depending on possible changes in vegetation**

453   **structure and to growing season length extension as a response to a changing climate (Lund et al., 2012; Ueyama et al.,**

454   **2014).**
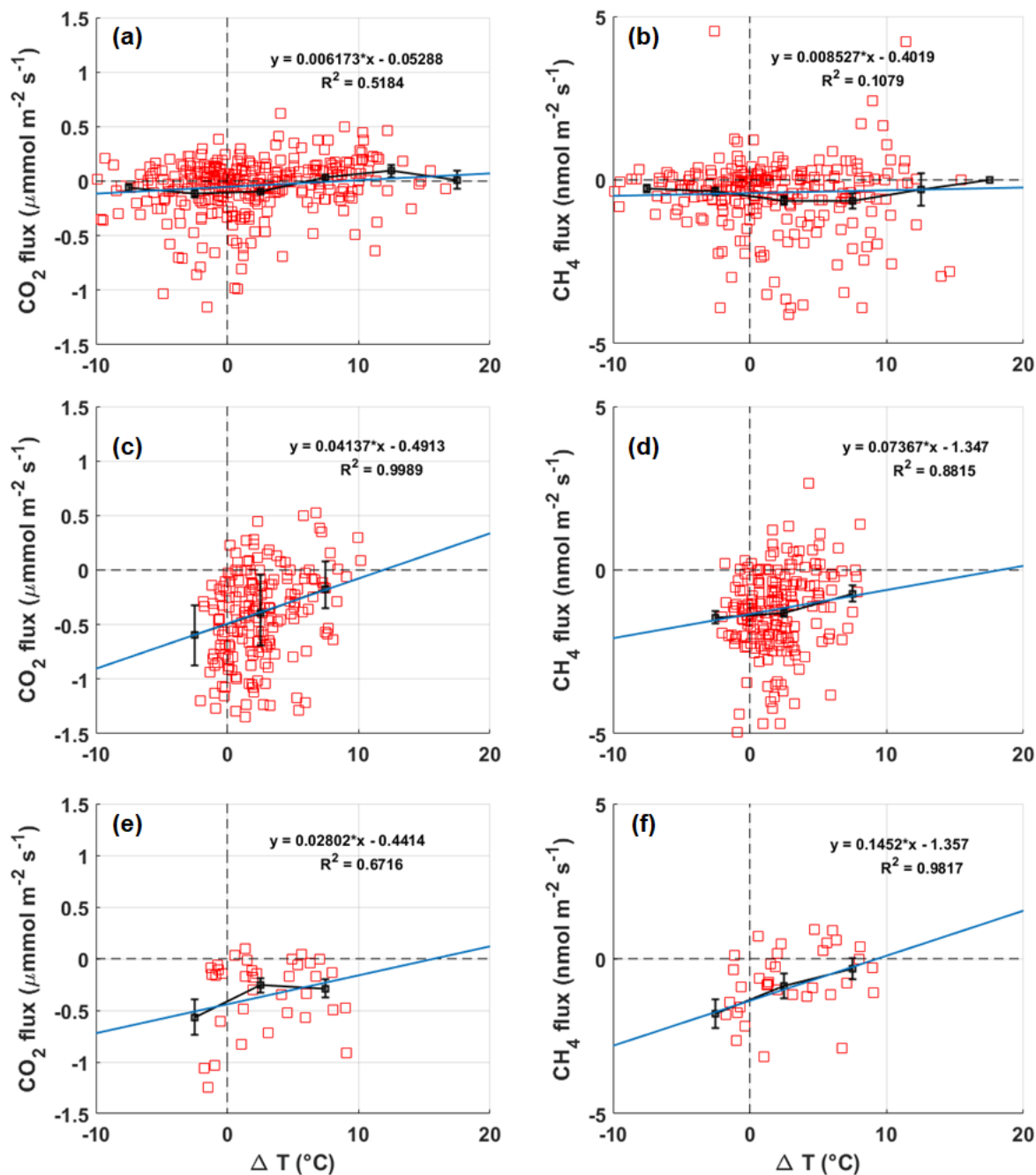
Figure 6 CO₂ vertical fluxes against temperature anomalies for (a) the whole winter (dark + light winter), (c) the summer and (e) the thawing season. CH₄ vertical fluxes against temperature anomalies for (b) the whole winter, (d) the summer and (f) the thawing season. A linear fit of the data is reported with a green line. Black squares represent the flux data binned for ΔT bins (5 °C large). Error bars represent the standard errors.

4. Conclusions

In this study, CO_2 and CH_4 turbulent fluxes on tundra ecosystems in the Svalbard Island (Norway) were investigated, using a two year-rounds measurement campaign. The observed **uptake**/emission patterns in both CO_2 and CH_4 underscore the dynamic interplay between climatic conditions and ecosystem activities (such as photosynthesis and microbial activity) at the measurement site. During the summer season, the pronounced uptake flux (for both carbon dioxide and methane) suggests an increase in mosses and lichens photosynthesis and/or microbial methane consumption, while the transition to neutral or null fluxes in the freezing season and in winter indicates a decrease in these activities. The enhanced methane uptake during the melting period aligns with the activation of soil microorganisms and correlates **with the increasing aeration (wind effect) of the topsoil and its decreasing albedo. The** CO_2 **uptake** intensified in the summer season, while during October the decreasing photosynthetic activity, together with the first occurrence of the snow, led to a sensible reduction of absorbing phenomena giving way to the ecosystem respiration and relatively low positive (or almost null) CO_2 fluxes. During the winter period the processes forcing CO_2 accumulation and CO_2 release counterbalance each other, resulting in very low positive fluxes. **Given the mineral-rich soils nature of the investigated area and of a large portion of the Arctic ecosystem, methane oxidation by aerobic methanotrophs in this kind of soils plays an important role in reducing the methane net emission to the atmosphere.** The methane budget shows a sink behaviour for this site, especially for the summer season gradually approaching neutral during the freezing season. The methane uptake decreases during the winter season due to the presence of the snow and the methanotrophic activity is nearly stopped by negative soil temperature, **which triggers the freezing process of the active layer water content.** Methane uptake rate rises again during the melting period started by the activation of soil methanotrophic microorganisms. **The CH_4 fluxes at CCT exhibited a limited association with both soil and ambient temperature in contrast to other environmental factors, such as the soil moisture and water table depth. In this work any soil hydrology measurements are available for understanding these processes, however the measured wind velocity and soil temperature have been used as proxies for soil moisture and water table depth. Solar radiation and wind play a role in the speed of drying, but the soil material and structure ultimately determine how much it dries under the given climatic conditions. Overall, the observed correlation in the ecosystem uptake of methane with wind velocity suggests that the methanotrophic communities in the Svalbard soils are stimulated by oxygen uptake, strongly related to its drying out during the summer.**

The analysis of the impact of thermal anomalies on CO_2 and CH_4 exchange fluxes, underscores that high positive (> 5 °C) thermal anomalies may contribute to an increased positive flux **both in summer and winter periods, effectively reducing the net annual uptake. Warming in permafrost ecosystems leads to increased plant and soil respiration that is initially compensated by an increased net primary productivity. However, future increases in soil respiration will likely outpace productivity, resulting in a positive feedback to climate change (Hicks Pries et al., 2013). In both cases, for methane and carbon dioxide, the uptake fluxes are generally observed for moderate positive anomalies (< 5°C), especially during summertime.** The implications of these results contribute valuable insights to our understanding of ecosystem responses in

493   the face of evolving climatic conditions. **If this trend is applicable also to other Arctic ecosystems, it will have implications**

494   **for our current understanding of Arctic ecosystems dynamics.** Further research is needed to better understand the sources

495   and sinks of these GHGs in the dry **upland tundra, to develop effective reference for models examining the dynamics of**

496   **these ecosystems in response to climate change, at local and global scale.**

497

498   **Appendix A: Climate Change Tower (CCT)**

499
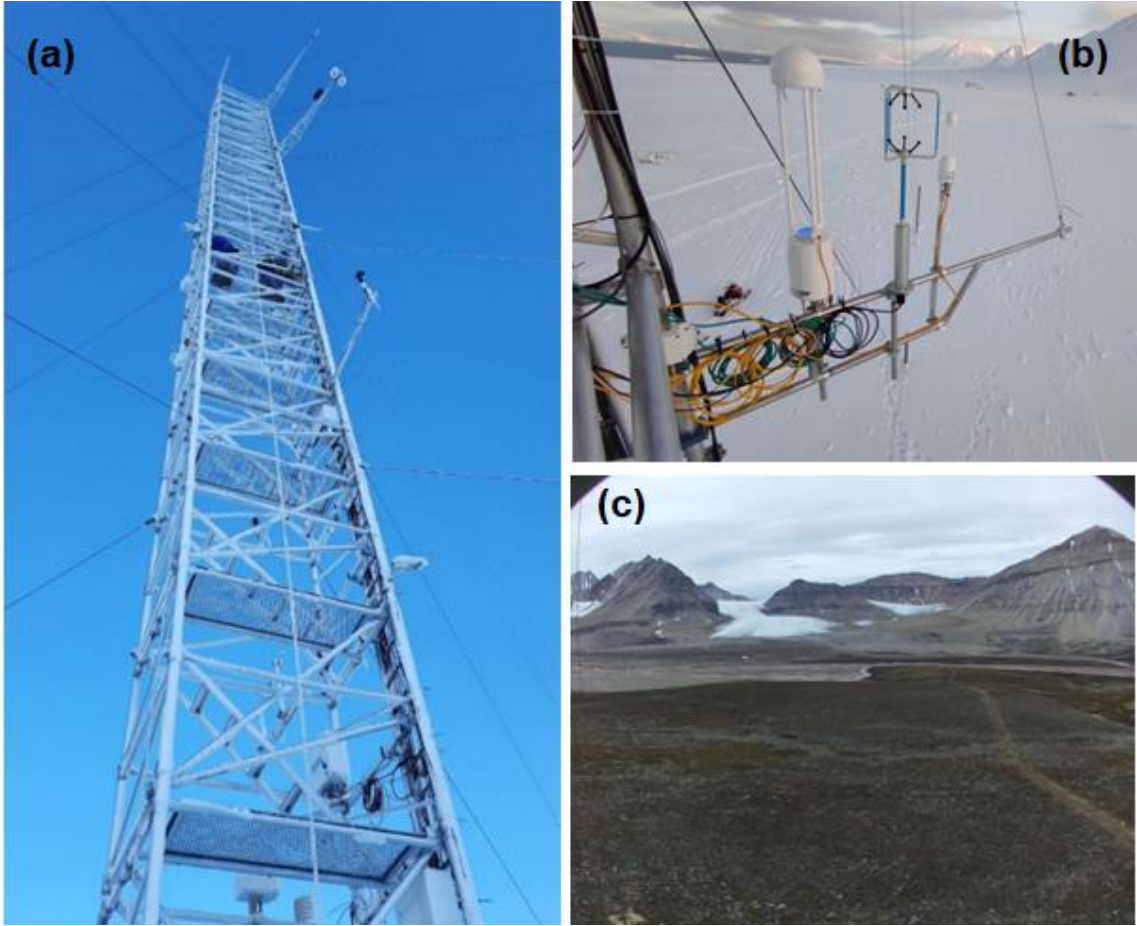
500   **Figure A1** (a) Climate Change Tower (CCT) picture with several instrumentations installed at different heights. (b) A picture
501   of the EC installation setup with Li7700 (left), sonic anemometer (middle) and Li7500A (right) on the steel horizontal bar. c)
502   A bird's-eye view of the tundra in the CCT site. Photo courtesy of Roberto Salzano (CNR-IIA).

503   **Appendix B: Meteorology at CCT for the measurement period**

504   The mean air temperature was of −1.3 °C (+/- 7 std. dev) during the measurement period. March records the lowest T, with a

505   daily average of -20.3 °C (see Fig. B1a), while from April onwards, T gradually rises, peaking at 13.5 °C daily in July. At the

506   same time, RH reached its maximum value of 93%, maintaining high levels throughout August (Fig. B1c). The minimum RH

value of 31% (on a daily basis) was recorded in April. Solar radiation (both global and net radiation) takes on positive values greater than 10 W m^{-2} from the month of February (starting halfway through) until the month of October (to about the 15th) (Fig. B1e). The total precipitation in the area for the two-year period was distributed as 235 mm in 2021 (from April to December), 573 mm in 2022 and 160 mm in 2023 (January-March only). **Total solar radiation (downward shortwave radiation),** which is one of the main drivers for the photosynthesis processes, showed relatively high median values for thawing and winter season **(510 W m^{-2} and 332 W m^{-2}, respectively), and decreasing values for summer (392 W m^{-2}) and freezing (240 W m^{-2}) (Fig. B1e).** Note that during dark winter the global radiation is very low, actually null, as this period has been defined. Snowpack in the first period until 27th of May 2021 had an average depth of 0.41 m with a maximum peak at 0.56 m in 2021. In 2022 and 2023 the depth of the snowpack was lower, with an average depth of 0.24 m and 0.14 m, respectively (Fig. 1b). The maximum snowpack depth in the last two years was 0.35 m. The snow is largely spread by wind, as is typical for such areas on Svalbard (Winther et al., 2003). Overall, the ground was covered by snow for 62% of the measurement period. The average difference between Ts at 5 cm and Ts at 10 cm was 0.006 °C, with an absolute average gradient over the whole period of 0.12 °C m^{-1} (Fig. 1b). The maximum Ts was 15 °C (in July), the minimum -16 °C (in December 2022). In this work a particular focus was placed on both the study of shoulder seasons as well as on winter and summer seasons. The temperature differences between the selected seasons were significant. Specifically, the winter period T (Fig. B1b) was sharply below zero (median -6.51 °C). The lowest cumulative precipitation (only rain) was observed in the freezing period (20 mm), while during the dark winter the total rainfall accounted for 522 mm, up to 53 mm on a daily basis, with four rain days for a total of 136 mm, corresponding to 26% of the dark winter total. Thawing period T was in milder conditions, with a median value of 2.92 °C (0.41-8.81 °C, min-max), while the warmest temperatures were observed during the summer season, even exceeding 5°C on median values (with a maximum of 13.47 °C) (Fig. B1b). Simple Daily Intensity Index (SDII) was calculated to provide information about the intensity of precipitation on days with rainfall. SDII computes the average amount of rainfall (mm) per day, offering a perspective on the strength of precipitation and indicating its intensity. Analysing the SDII index (Lucas et al., 2021), the thawing period recorded the highest value (7.4 mm day-1) with an absolute rainfall of 37 mm, followed by the dark winter period (6.6 mm day-1), while the lowest value (2.9 mm d-1) was observed during the freezing period, suggesting lighter rainfall on rainy days (Fig. B1h). High RH conditions (up to a median of 72 %) were prevailing during the summer season (Fig. B1d) with a cumulative precipitation of 230 mm (SDII 5.6 mm d-1). The freezing period was generally characterised by temperatures that can reach a median of -4.35 °C in October, with RH reaching a minimum of 46 %.

536

537

538
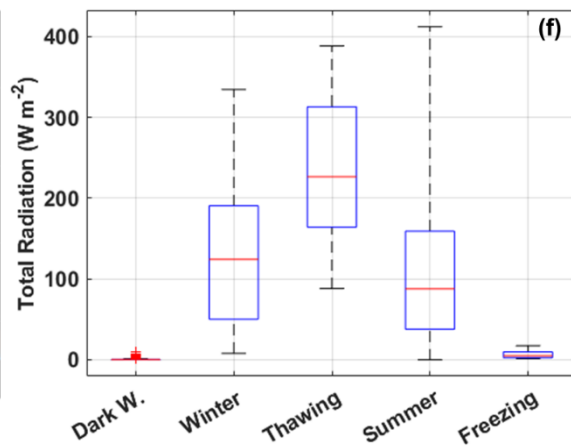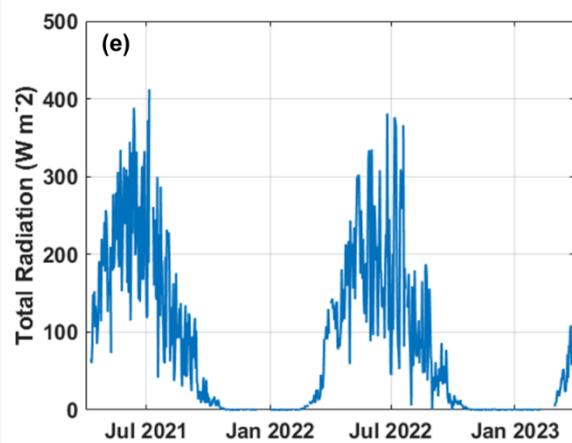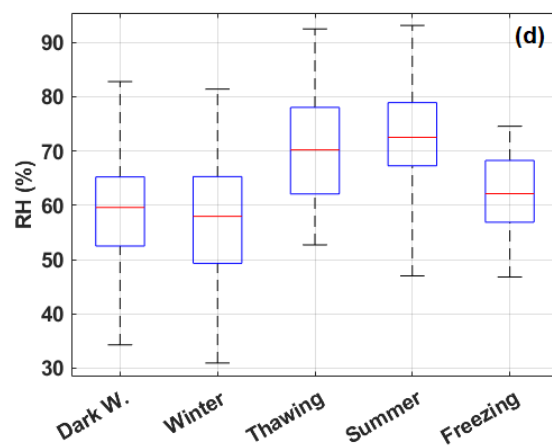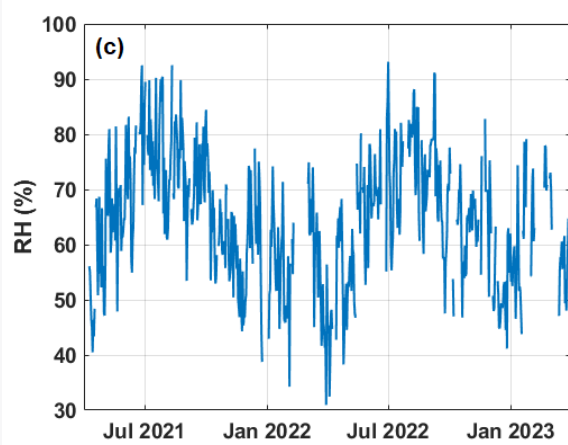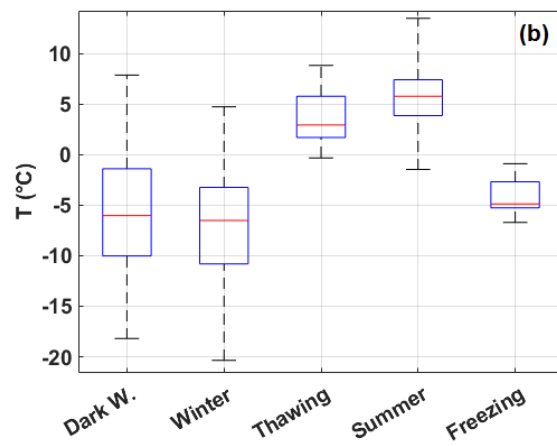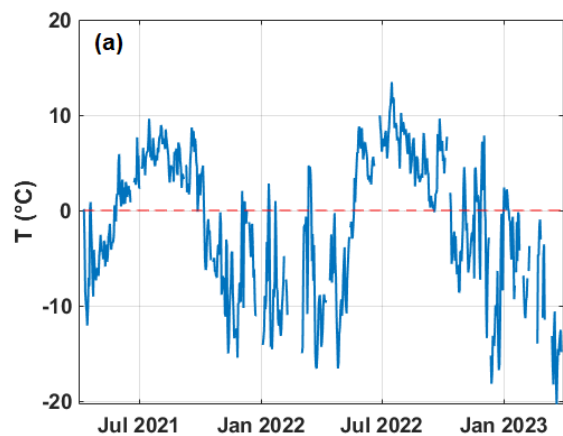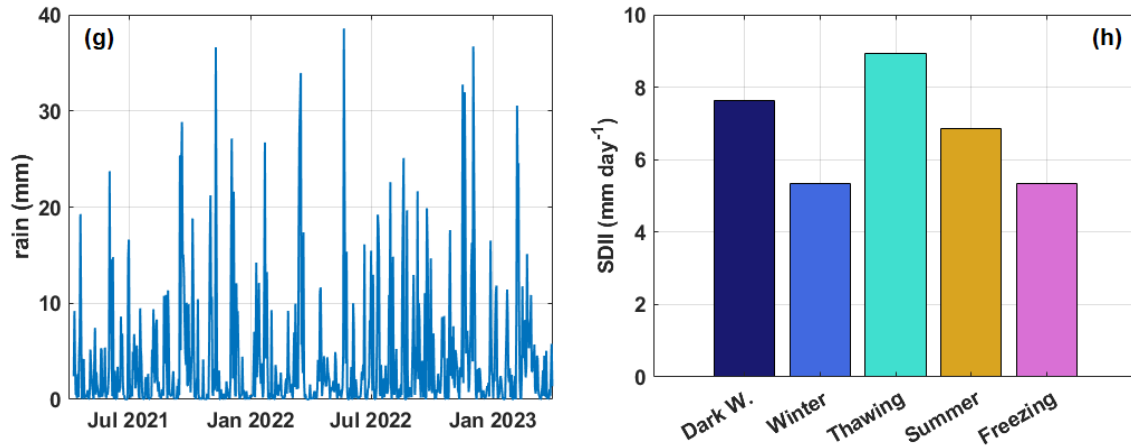
Figure B1 Time series and box plot with whiskers on daily and seasonal basis respectively of (a-b) temperature (°C); (c-d) relative humidity (%); (e) **total radiation (downward shortwave radiation)** (W m⁻²) and (f) SDII (mm d⁻¹) at CCT site. In the right panels, whiskers represent max and min values, the box limits are the 25th and 75th percentiles. The red line represents the median value on a 30 min basis.

Appendix C: Micrometeorology at CCT for the measurement period

In the measurement period, sensible heat flux was on average negative (- 6 W m⁻²), on a daily basis (Fig. C1a). The results show the presence of a long period with negative energy fluxes from freezing to thawing season and a minimum around -77 W m⁻² until snow cover was present and during the melting snow phase, when the atmosphere was warmer than the surface. Sensible heat flux values had a positive magnitude (directed toward the atmosphere) for 32.7% of cases and for 67.3% of events it was directed toward the snowpack. Upon thawing, a positive sensible heat flux became evident (see Fig. C1b), exhibiting median values of 4.2 W m⁻² (max 47 W m⁻²) in July, corresponding to the peak net solar radiation (253 W m⁻²) observed throughout the year. This behaviour had previously been observed in the Arctic (Kral et al., 2014; Donateo et al., 2023) where the snowpack acts as a sink of heat during the winter and spring months. In the freezing period, sensible heat fluxes were negative (median -6.04 W m⁻²), down to -26 W m⁻² on daily averages, indicating energy moving toward the surface (Fig. C1b). Latent heat flux (Fig. C1c,d) had its minimum median value during the winter (light winter with a median of 1.19 W m⁻²), while its maximum median on season basis was reached during the summer (14.32 W m⁻²). Intermediate values were registered during the shoulder seasons, with 1.19 W m⁻² and 2.4 W m⁻² during thawing and freezing, respectively. In general, in this dataset no significant correlation between methane and latent heat fluxes has been observed (not shown here). Latent heat flux was positive for 76.2% of the cases, while it was directed toward the soil in 23.7% of cases. The median measured latent heat flux was 2.93 W m⁻² (8.48 W m⁻² on average) during the observation campaign. In Fig. C1e the time series of friction velocity shows a mean value of 0.19 m s⁻¹ on the whole measurement period. No specific differences can be noted in the friction velocity behaviour due to the changing in snowpack characteristics or through the selected seasons. During winter, the friction velocity oscillated around a median value of 0.16 m s⁻¹. Thawing median value was slightly lower (about 0.13 m

563   s⁻¹), while during summer the maximum values reached 0.15 m s⁻¹ (Fig. C1f). In particular, the frequency of stable and highly

564   stable atmospheric conditions is 54% and 13%, respectively, of the total cases; while unstable and highly unstable conditions

565   occur for 20% and 12%, respectively. Finally, neutral conditions were rare, showing a frequency below 1%. Atmospheric

566   stable conditions prevailed for the whole year, especially during the Arctic night (with a maximum stability parameter of 1.8).

567   During dark and winter seasons, stable and very stable conditions were predominant (65% and 16%, respectively). Unstable

568   atmospheric conditions arose only during the summer period with a median stability parameter of 0.47. In summer, there was

569   a prevalence of unstable (33%) and very unstable (20%) conditions, with very stable cases below 10%. The thawing season

570   also exhibited a predominant stable situation (with 69% of stable and very stable cases) with a median stability parameter of

571   0.22. The freezing season showed a stability frequency distribution like the previous shoulder season, with a higher prevalence

572   of stable cases (60%).

573

574
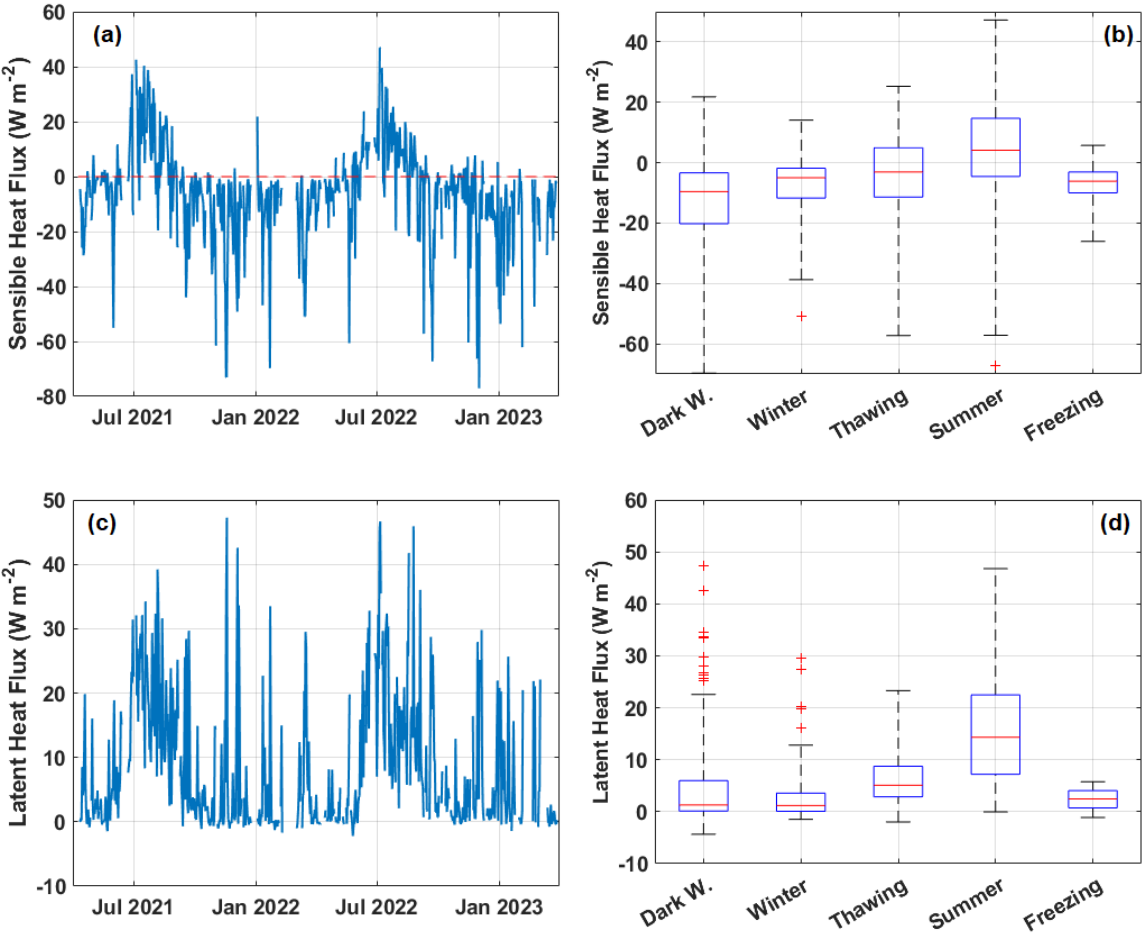
575
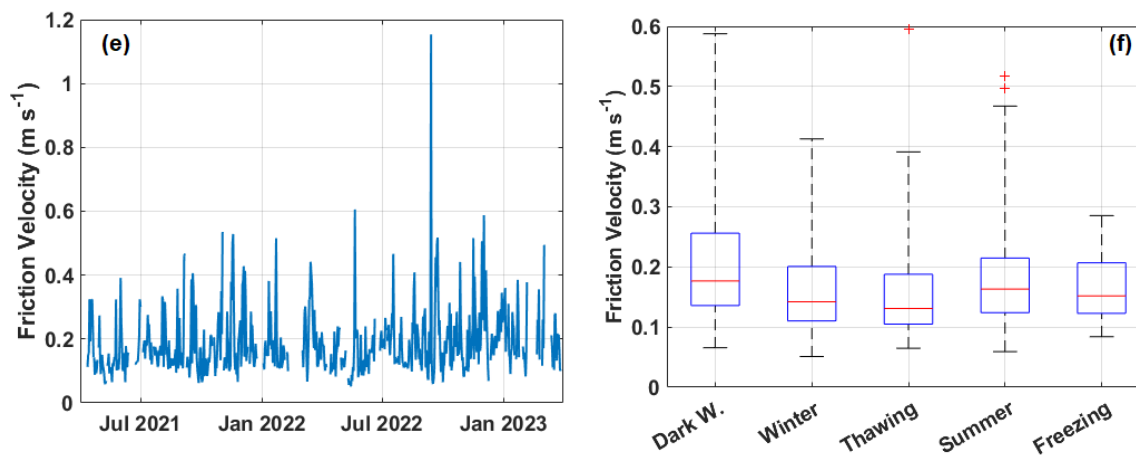
Figure C1 Time series on a daily basis (left) and whiskers-box plots (right) of the principal micrometeorological variables measured during the campaign. (a,b) Sensible heat flux (W m^{-2}); (c,d) latent heat flux (W m^{-2}) and (e,f) friction velocity (m s^{-1}). In the right panels, whiskers represent max and min values, the box limits are the 25th and 75th percentiles. The red line represents the median value on a 30 min basis.

Data availability: The data that support the findings of this study are openly available in the Italian Arctic Data Center (IADC) at https://doi.org/10.48230/DSET.2024.0001 (Donateo et al., 2024).

Author contributions: **AD**: Conceptualization; instrumental setup, data collection and post-processing, data curation; formal analysis; investigation; methodology; visualisation; writing – original draft, funding acquisition; project administration; supervision. **DF**: data curation; formal analysis; investigation; methodology; writing – review and editing. **DG**: Investigation; methodology; writing – review and editing. **AM**: Data curation; formal analysis; investigation; methodology; writing – review and editing. **MM**: Instrumental setup, data collection and post-processing, data curation; writing – review and editing. **SD**: investigation; methodology; writing – review and editing, funding acquisition; project administration; **GP**: Conceptualization; instrumental setup, data collection and post-processing, data curation; formal analysis; investigation; methodology; visualisation; writing – original draft.

Competing interests: The authors declare that they have no conflict of interest.

Acknowledgements: This work has been conducted in the framework of the Joint Research Agreement ENI-CNR, WP1 "Impatto delle emissioni in atmosfera sulla criosfera e sul cambiamento climatico nell'Artico". The Authors wish to thank the staff of CNR-ISP for the logistical support at Arctic Station "Dirigibile Italia" in Ny Ålesund. **Further, the Authors wish to thank the two anonymous Reviewers whose comments helped to improve this paper.**

References

AMAP, 2021. AMAP Assessment 2021: Impacts of Short-lived Climate Forcers on Arctic Climate, Air Quality, and Human Health. Arctic Monitoring and Assessment Programme (AMAP), Tromsø, Norway. x + 375pp. ISBN – 978-82-7971-202-2.

Arndt, K. A., Oechel, W. C., Goodrich, J. P., Bailey, B. A., Kalhori, A., Hashemi, J., Sweeney, C., and Zona, D.: Sensitivity of methane emissions to later soil freezing in Arctic tundra ecosystems, J. Geoph. Res.: Biogeosciences, 124 (8), 2595–2609, https://doi.org/10.1029/2019J G005242, 2019.

Arnold, S. R., Law, K. S., Brock, C. A., Thomas, J. L., Starkweather, S. M., von Salzen, K., Stohl, A., Sharma, S., Lund, M. T., Flanner, M.G., Petäjä, T., Tanimoto, H., Gamble, J., Dibb, J. E., Melamed, M., Johnson, N., Fidel, M., Tynkkynen, V. -P., Baklanov, A., Eckhardt, S., Monks, S. A., Browse, J., Bozem, H.: Arctic air pollution: Challenges and opportunities for the next decade, Elementa: Science of the Anthropocene, 4, 104, https://doi.org/10.12952/journal.elementa.000104, 2016.

Aubinet, M., Vesala, T., Papale, D., et al.: Eddy Covariance. A Practical Guide to Measurement and Data Analysis, Springer Atmospheric Sciences, https://doi.org/10.1007/978-94-007-2351-1, 2012.

Bao, T., Xu, X., Jia, G., Billesbach, D. P., and Sullivan, R. C.: Much stronger tundra methane emissions during autumn freeze than spring thaw, Global Change Biol., 27, 376–387, https://doi.org/10.1111/gcb.15421, 2021.

Bintanja, R., and Van der Linden, E. C.: The changing seasonal climate in the Arctic, Sci Rep-UK, 3, 1556, https://doi.org/10.1038/srep01556, 2013.

Boike, J., Juszak, I., Lange, S., Chadburn, S., Burke, E., Overduin, P.P., Roth, K., Ippisch, O., Bornemann, N., Stern, L., Gouttevin, I., Hauber, E., and Westermann, S.: A 20-year record (1998–2017) of permafrost, active layer and meteorological conditions at a high Arctic permafrost research site (Bayelva, Spitsbergen). Earth Syst. Sci. Data, 10, 355–390, https://doi.org/10.5194/essd-10-355-2018, 2018

Burba, G., McDermitt, D. K., Grelle, A., Anderson, D., and Xu, L.: Addressing the influence of instrument surface heat exchange on the measurements of CO_2 flux from open-path gas analyzers, Global Change Biol., 14, 1854–1876, https://doi.org/10.1111/j.1365-2486.2008.01606.x, 2008.

Cahoon, S. M. P., Sullivan, P. F., Post, E., and Welker, J. M.: Large herbivores limit CO_2 uptake and suppress carbon cycle responses to warming in West Greenland, Global Change Biol., 2, 469–479, https://doi.org/10.1111/j.1365-2486.2011.02528.x, 2012.

Christiansen, J. R., Romero, A. J. B., Jørgensen, N. O. G., Glaring, M. A., Jørgensen, C. J., Berg, L. K., and Elberling, B.: Methane fluxes and the functional groups of methanotrophs and methanogens in a young Arctic landscape on Disko Island, West Greenland, Biogeochemistry 122, 15–33, https://doi.org/10.1007/s10533-014-0026-7, 2015.

Cicerone, R. J., and Oremland, R. S.: Biogeochemical aspects of atmospheric methane, Global Biogeochem. Cy. 2, 299–327, https://doi.org/10.1029/GB002i004p00299, 1988.

Curry, C.: Modelling the soil consumption of atmospheric methane at the global scale, Global Biogeochem. Cy., 21, GB4012, https://doi.org/10.1029/2006GB002818, 2007.

D'Imperio, L., Li, B.-B., Tiedje, J. M., Oh, Y., Christiansen, J. R., Kepfer-Rojas, S., Westergaard-Nielsen, A., Brandt, K. K., Holm, P. E., Wang, P., Ambus, P., and Elberling, B.: Spatial controls of methane uptake in upland soils across climatic and geological regions in Greenland. Communications Earth & Environment, 4(1), 461. https://doi.org/10.1038/s43247-023-01143-3, 2023

D'Imperio, L., Nielsen, C. S., Westergaard-Nielsen, A., Michelsen, A., and Elberling, B.: Methane oxidation in contrasting soil types: responses to experimental warming with implication for landscape-integrated CH_4 budget, Global Change Biol. 23, 966–976, https://doi.org/10.1111/gcb.13400, 2017.

Donateo, A., Famulari, D., Giovannelli, D., Mariani, A., Mazzola, M., Decesari, S., Pappaccogli, G.: Observations of methane net sinks in the Arctic tundra – Data, Italian Arctic Data Center (IADC), https://doi.org/10.48230/DSET.2024.0001, 2024.

Donateo, A., Pappaccogli, G., Famulari, D., Mazzola, M., Scoto, F., and Decesari, S.: Characterization of size-segregated particles turbulent flux and deposition velocity by eddy correlation method at an Arctic site, Atmos. Chem. Phys., 23, 7425–7445, https://doi.org/10.5194/acp-23-7425-2023, 2023.

Dutaur, L., and Verchot, L.V.: A global inventory of the soil CH_4 sink. Global Biogeochem. Cycles, 21, 4013. https://doi.org/10.1029/2006GB002734, 2007.

Dyukarev, E.: Comparison of Artificial Neural Network and Regression Models for Filling Temporal Gaps of Meteorological Variables Time Series, Appl. Sci. 13, 2646, https://doi.org/10.3390/app13042646, 2023.

Emmerton, C. A., St Louis, V. L., Lehnherr, I., Graydon, J. A., Kirk, J. L., and Rondeau, K. J.: The importance of freshwater systems to the net atmospheric exchange of carbon dioxide and methane with a rapidly changing high Arctic watershed, Biogeosciences, 13, 5849–5863, https://doi.org/10.5194/bg-13-5849-2016, 2016.

Emmerton, C. A., St Louis, V. L., Lehnherr, I., Humphreys, E. R., Rydz, E., and Kosolofski, H. R.: The net exchange of methane with high Arctic landscapes during the summer growing season, Biogeosciences, 11, 3095–3106, https://doi.org/10.5194/bg-11-3095-2014, 2014.

Euskirchen, E. S., Bret-Harte, M. S., Scott, G. J., Edgar, C., and Shaver, G. R.: Seasonal patterns of carbon dioxide and water fluxes in three representative tundra ecosystems in northern Alaska, Ecosphere, 3(1):4, http://dx.doi.org/10.1890/ES11-00202.1, 2012.

Finkelstein, P. L., and Sims, P. F.: Sampling error in eddy correlation flux measurements, J. Geophys. Res-Atmos., 106, 3503–3509, https://doi.org/10.1029/2000JD900731, 2001.

Fratini, G., McDermitt, D. K., and Papale, D.: Eddy-covariance flux errors due to biases in gas concentration measurements: origins, quantification and correction, Biogeosciences, 11, 1037–1051, https://doi.org/10.5194/bg-11-1037-2014, 2014.

Gash, J. H. C., and Culf, A. D.: Applying a linear detrend to eddy correlation data in real time, Bound-Lay. Meteorol., 79(3), 301 – 306, https://doi.org/10.1007/BF00119443, 1996.

Hicks Pries, C.E., Schuur, E.A.G. and Crummer, K.G.: Thawing permafrost increases old soil and autotrophic respiration in tundra: Partitioning ecosystem respiration using d13C and Δ14C. Glob. Change Biol., 19, 649–661, doi: 10.1111/gcb.12058, 2013

Hodson, A. J., Nowak, A., Redeker, K. R., Holmlund, E. S., Christiansen, H. H., and Turchyn, A. V.: Seasonal dynamics of methane and carbon dioxide evasion from an open system pingo: Lagoon Pingo, Svalbard, Front. Earth Sci. 7:30, https://doi.org/10.3389/feart.2019.00030, 2019.

Horst, T. W., and Lenschow, D. H.: Attenuation of scalar fluxes measured with spatially-displaced sensors, Bound-Lay. Meteorol., 130, 275-300, https://doi.org/10.1007/s10546-008-9348-0, 2009.

Howard, D., Agnan, Y., Helmig, D., Yang, Y., and Obrist, D.: Environmental controls on ecosystem-scale cold-season methane and carbon dioxide fluxes in an Arctic tundra ecosystem. Biogeosciences, 17, 4025–4042, https://doi.org/10.5194/bg-17-4025-2020, 2020.

Howarth, R. W., Santoro, R., and Ingraffea, A.: Methane and the greenhouse gas footprint of natural gas from shale formations, Climatic Change, https://doi.org/10.1007/s10584-011-0061-5, 2011.

Hugelius, G., Strauss, J., Zubrzycki, S., Harden, J. W., Schuur, E. A. G., Ping, C.-L., Schirrmeister, L., Grosse, G., Michaelson, G. J., Koven, C. D., O'Donnell, J. A., Elberling, B., Mishra, U., Camill, P., Yu, Z., Palmtag, J., and Kuhry, P.: Estimated stocks of circumpolar permafrost carbon with quantified uncertainty ranges and identified data gaps, Biogeosciences, 11, 6573–6593, https://doi.org/10.5194/bg-11-6573-2014, 2014.

Kim, Y., Johnson, M. S., Knox, S. H., Black, T. A., Dalmagro, H. J., Kang, M., Kim, J., and Baldocchi, D.: Gap-filling Approaches for Eddy Covariance Methane Fluxes: A Comparison of Three Machine Learning Algorithms and a Traditional Method with Principal Component Analysis, Global Change Biol., 26, 1499–1518, https://doi.org/10.1111/gcb.14845, 2020.

Kljun, N., Calanca, P., Rotach, M. W., and Schmid, H. P.: A simple two-dimensional parameterisation for Flux Footprint Prediction (FFP), Geosci. Model Dev., 8, 3695–3713, https://doi.org/10.5194/gmd-8-3695-2015, 2015.

Knoblauch, C., Beer, C., Liebner, S., Grigoriev, M. N., and Pfeiffer, E.: Methane production as key to the greenhouse gas budget of thawing permafrost, Nature Clim. Change, 8, 309–312, https://doi.org/10.1038/s41558-018-0095-z, 2018.

Knox, S. H., Bansal, S., McNicol, G., Schafer, K., Sturtevant, C., Ueyama, M., Valach, A. C., Baldocchi, D., Delwiche, K., Desai, A. R., Euskirchen, E., Liu, J., Lohila, A., Malhotra, A., Melling, L., Riley, W., Runkle, B. R. K., Turner, J., Vargas, R., Zhu, Q., Alto, T., Chouinard, E., Goeckede, M., Melton, J. R., Sonnentag, O., Vesala, T., Ward, E., Zhang, Z., Feron, S., Ouyang, Z., Alekseychik, P., Aurela, M., Bohrer, G., Campbell, D. I., Chen, J., Chu, H., Dalmagro, H. J., Goodrich, J. P., Gottschalk, P., Hirano, T., Iwata, K., Jurasinski, G., Kang, M., Koebsch, F., Mammarella, I., Nilsson, M. B., Ono, K., Peichl, M., Peltola, O., Ryu, Y., Sachs, T., Sakabe, A., Sparks, J. P., Tuittila, E., Vourlitis, G. L., Wong, G. X., Windham-Myers, L., Poulter, B., and Jackson, R. B.: Identifying dominant environmental predictors of freshwater wetland methane fluxes across diurnal to seasonal time scales, Global Change Biol., 27, 3582–3604, https://doi.org/10.1111/gcb.15661, 2021.

Kral, S. T., Sjöblom, A., and Nygård, T.: Observations of summer turbulent surface fluxes in a High Arctic fjord, Q. J. Roy. Meteorol. Soc., 140: 666–675, https://doi.org/10.1002/qj.2167, 2014.

Juncher Jørgensen, C., Schlaikjær Mariager, T., and Riis Christiansen, J.: Spatial variation of net methane uptake in Arctic and subarctic drylands of Canada and Greenland. Geoderma, 443, 116815. https://doi.org/10.1016/j.geoderma.2024.116815, 2024

Juncher Jørgensen, C., Lund Johansen, K. M., Westergaard-Nielsen, A., and Elberling, B.: Net regional methane sink in High Arctic soils of northeast Greenland, Nat. Geosci., 8, 20–23, https://doi.org/10.1038/ngeo2305, 2015.

Intergovernmental Panel on Climate Change (IPCC) (2023) Climate Change 2021 – The Physical Science Basis: Working Group I Contribution to the Sixth Assessment Report of the Intergovernmental Panel on Climate Change. Cambridge: Cambridge University Press.

Ishizawa, M., Chan, D., Worthy, D., Chan, E., Vogel, F., and Maksyutov, S.: Analysis of atmospheric CH_4 in Canadian Arctic and estimation of the regional CH_4 fluxes, Atmos. Chem. Phys., 19, 4637–4658, https://doi.org/10.5194/acp-19-4637-2019, 2023.

Yun, J., Yang, Y., Zhou, X., Lee, J., Choi, J., Kim, M., Gyeong, H., Laffly, D., and Kang, D.: Effects of deglaciation on the succession of methanotrophic communities in inland and tidewater glaciers in the high Arctic, Svalbard, Catena, 231.107267, https://doi.org/10.1016/j.catena.2023.107267, 2023.

Lafleur, P. M., and Humphreys, E. R.: Spring warming and carbon dioxide exchange over low Arctic tundra in central Canada, Global Change Biol., 14, 740–756, https://doi.org/10.1111/j.1365-2486.2007.01529.x, 2007.

Lara, M. J., Nitze, I., Grosse, G., Martin, P., and McGuire, A. D.: Reduced arctic tundra productivity linked with landform and climate change interactions, Sci. Rep. 8, 2345, https://doi.org/10.1038/s41598-018-20692-8, 2018.

Lau, M. C. Y., Stackhouse, B. T., Layton, A. C., Chauhan, A., Vishnivetskaya, T. A., Chourey, K., Ronholm, J., Mykytczuk, N. C. S., Bennett, P. C., Lamarche-Gagnon, G., Burton, N., Pollard, W. H., Omelon, C. R., Medvigy, D. M., Hettich, R. L., Pfiffner, S. M., Whyte, L. G., and Onstott, T. C.: An active atmospheric methane sink in high Arctic mineral cryosols, ISME J., 9, 1880-1891, 2015.

Law, K. S., Stohl, A., Quinn, P. K., Brock, C. A., Burkhart, J. F., Paris, J.-D., Ancellet, G., Singh, H. B., Roiger, A., Schlager, H., Dibb, J., Jacob, D. J., Arnold, S. R., Pelon, J., and Thomas, J. L.: Arctic air pollution: New insights from POLARCAT-IPY, B. Am. Meteorol. Soc., 95(12), 1873–1895, https://doi.org/10.1175/bams-d-13-00017.1, 2014.

Lindroth, A., Pirk, N., Jónsdóttir, I. S., Stiegler, C., Klemedtsson, L., and Nilsson, M. B.: CO_2 and CH_4 exchanges between moist moss tundra and atmosphere on Kapp Linné, Svalbard, Biogeosciences, 19, 3921–3934, https://doi.org/10.5194/bg-19-3921-2022, 2022.

Lloyd, C. R., Harding, R. J., Friborg, T., and Aurela, R.: Surface fluxes of heat and water vapour from sites in the European Arctic, Theor. Appl. Climatol., 70, 19–33, https://doi.org/10.1007/s007040170003, 2001.

Lüers, J., Westermann, S., Piel, K., and Boike, J.: Annual CO_2 budget and seasonal CO_2 exchange signals at a high Arctic permafrost site on Spitsbergen, Svalbard archipelago, Biogeosciences, 11, 6307–6322, https://doi.org/10.5194/bg-11-6307-2014, 2014.

Lucas, E. W. M., de Sousa, F. de A. S., dos Santos Silva, F. D., Lins da Rocha Jr, R., Cavalcante Pinto, D. D., and de Paulo Rodrigues da Silva, V.: Trends in climate extreme indices assessed in the Xingu river basin - Brazilian Amazon, Weather and Climate Extremes, 31, 100306, https://doi.org/10.1016/j.wace.2021.100306, 2021.

Magnani, M., Baneschi, I., Giamberini, M., Raco, M., and Provenzale, A.: Microscale drivers of summer CO_2 fluxes in the Svalbard High Arctic tundra, Sci. Rep., 12:763, https://doi.org/doi.org/10.1038/s41598-021-04728-0, 2022.

Massmann, W. J.: Reply to comment by Rannik on "A simple method for estimating frequency response corrections for eddy covariance systems", Agr. For. Meteor., 107, 247–251, https://doi.org/10.1016/S0168-1923(00)00237-9, 2001.

Massmann, W. J.: A simple method for estimating frequency response corrections for eddy covariance systems, Agr. For. Meteor., 104, 3, 185-198, https://doi.org/10.1016/S0168-1923(00)00164-7, 2000.

Mastepanov, M., Sigsgaard, C., Tagesson, T., Ström, L., Tamstorf, M. P., Lund, M., and Christensen, T. R.: Revisiting factors controlling methane emissions from high-Arctic tundra, Biogeosciences, 10, 5139–5158, https://doi.org/10.5194/bg-10-5139-2013, 2013.

Mastepanov, M., Sigsgaard, C., Dlugokencky, E. J., Houweling, S., Strom L., Tamstorf, M. P., and Christensen, T. R.: Large tundra methane burst during onset of freezing, Nature, 456, 628–631, https://doi.org/10.1038/nature07464, 2008.

Mauder, M., Cuntz, M., Drüe, C., Graf, A., Rebmann, C., Schmid, H. P., Schmidt, M., and Steinbrecher, R.: A strategy for quality and uncertainty assessment of long-term eddy-covariance measurements, Agr. For. Meteor., 169, 122–135, https://doi.org/10.1016/j.agrformet.2012.09.006, 2013.

Mauder, M., and Foken, T.: Documentation and instruction manual of the eddy covariance software package TK2, Arbeitsergebnisse, Universitat at Bayreuth, Abt. Mikrometeorologie 26, 45, 2004.

Mazzola, M., Viola, A. P., Choi, T., and Tampieri, F.: Characterization of Turbulence in the Neutral and Stable Surface Layer at Jang Bogo Station, Antarctica, Atmosphere, 12, 1095, https://doi.org/10.3390/atmos12091095, 2021.

Mazzola, M., Tampieri, F., Viola, A. P., Lanconelli, C., and Choi, T.: Stable boundary layer vertical scales in the Arctic: observations and analyses at Ny-Ålesund, Svalbard, Q. J. Roy. Meteor. Soc., 142: 1250–1258, https://doi.org/10.1002/qj.2727, 2016.

McDermitt, D., Burba, G., Xu, L., Anderson, T., Komissarov, A., Riensche, B., Schedlbauer, J., Starr, G., Zona, D., Oechel, W., Oberbauer, S., and Hastings, S.: A new low-power, open-path instrument for measuring methane flux by eddy covariance, Appl. Phys. B 102, 391–405, https://doi.org/10.1007/s00340-010-4307-0, 2011.

Moncrieff, J., Clement, R., Finnigan, J., and Meyers, T.: Averaging, detrending, and filtering of eddy covariance time series, Handbook of Micrometeorology. pp. 7 – 31, https://doi.org/10.1007/1-4020-2265-4_2, 2004.

Nakai, T., Van der Molen, M., Gash, J., and Kodama, Y.: Correction of sonic anemometer angle of attack errors, Agr. For. Meteor., 136(1), 19–30, https://doi.org/10.1016/j.agrformet.2006.01.006, 2006.

Oechel, W. C., Laskowski, C. A., Burba, G., Gioli, B. , and Kalhori, A. A. M.: Annual patterns and budget of CO_2 flux in an Arctic tussock tundra ecosystem. J. Geophys. Res. Biogeosci., 119, 323–339, doi:10.1002/2013JG002431, 2014.

Oh, Y., Zhuang, Q., Liu, L., Welp, L. R., Lau, M. C. Y., Onstott, T. C., Medvigy, D., Bruhwiler, L., Dlugokencky, E. J., Hugelius, G., D'Imperio, L., and Elberling, B.: Reduced net methane emissions due to microbial methane oxidation in a warmer Arctic, Nature Clim. Change, vol. 10, 317–321, https://doi.org/10.1038/s41558-020-0734-z, 2020.

Ohtsuka, T., Adachi, M., Uchida, M., and Nakatsubo, T.: Relationships between vegetation types and soil properties along a topographical gradient on the northern coast of the Brøgger Peninsula, Svalbard, Polar Biosci., 19, 63–72, oai:nipr.repo.nii.ac.jp:00006240, 2006.

Papale, D., Reichstein, M., Aubinet, M., Canfora, E., Bernhofer, C., Kutsch, W., Longdoz, B., Rambal, S., Valentini, R., Vesala, T., and Yakir, D.: Towards a standardized processing of Net Ecosystem Exchange measured with eddy covariance technique: algorithms and uncertainty estimation, Biogeosciences, 3(4), 571-583, https://doi.org/10.5194/bg-3-571-2006, 2006.

Pedregosa, F., Varoquaux, G., Gramfort, A., Michel, V., Thirion, B., Grisel, O., Blondel, M., Prettenhofer, P., Weiss, R., Dubourg, V., Vanderplas, J., Passos, A., Cournapeau, D., Brucher, M., Perrot, M., and Duchesnay, E.: Scikit-learn: Machine Learning in Python, J. Mach. Learn. Res., 12, 2825–2830, https://doi.org/10.5555/1953048.2078195, 2011.

Pirk, N., Tamstorf, M. P., Lund, M., Mastepanov, M., Pedersen, S. H., Mylius, M. R., Parmentier, F.-J., Christiansen, H. H., and Christensen, T. R.: Snowpack fluxes of methane and carbon dioxide from high Arctic tundra, J. Geophys. Res.-Biogeo., 121(11), 2886–2900, https://doi.org/10.1002/2016j g003486, 2016.

848 Pirk, N., Santos, T., Gustafson, C., Johansson, A. J., Tufvesson, F., Parmentier, F.-J., Mastepanov, M., and Christensen, T. R.:
849 Methane emission bursts from permafrost environments during autumn freeze-in: New insights from ground-penetrating radar,
850 Geophys. Res. Lett., 42(16), 6732–6738, https://doi.org/10.1002/2015G L065034, 2015.
851
852 Reay, D., Hewitt, C. N., Smith, K., and Grace, J.: Greenhouse Gas Sinks, CABI, Oxfordshire, ISBN 978-1-84593-189-6, 2007.
853
854 Reichstein, M., Falge, E., Baldocchi, D., Papale, D., Aubinet, M., Berbigier, P., Bernhofer, C., Buchmann, N., Gilmanov, T.,
855 Granier, A., Grünwald, T., Havránková, K., Ilvesniemi, H., Janous, D., Knohl, A., Laurila, T., Lohila, A., Loustau, D.,
856 Matteucci, G., Meyers, T., Miglietta, F., Ourcival, J.-M., Pumpanen, J., Rambal, S., Rotenberg, E., Sanz, M., Tenhunen, J.,
857 Seufert, G., Vaccari, F., Vesala, T., Yakir, D., and Valentini, R.: On the separation of net ecosystem exchange into assimilation
858 and ecosystem respiration: review and improved algorithm, Global Change Biol., 11, 1424–1439,
859 https://doi.org/10.1111/j.1365-2486.2005.001002.x, 2005.
860
861 Sand, M., Berntsen, T. K., von Salzen, K., Flanner, M. G., Langner, J., and Victor, D. G.: Response of Arctic temperature to
862 changes in emissions of short-lived climate forcers, Nature Clim. Change, 6(3), 286–289,
863 https://doi.org/10.1038/nclimate2880, 2015.
864
865 Schmale, J., Zieger, P., and Ekman, A. M. L.: Aerosols in current and future Arctic climate, Nat. Clim. Change, 11, 95–105,
866 https://doi.org/10.1038/s41558-020-00969-5, 2021.
867
868 **Serrano-Ortiz, P., Kowalski, A. S., Domingo, F., Ruiz, B. and Alados-Arboledas, L.: 2008: Consequences of**
869 **uncertainties in CO_2 density for estimating net ecosystem CO_2 exchange by open-path eddy covariance. Bound.-Layer**
870 **Meteor., 126, 209-218, https://doi.org/10.1007/s10546-007-9234-1.**
871
872 Serrano-Silva, N., Sarria-Guzman, Y., Dendooven, L., and Luna-Guido, M.: Methanogenesis and methanotrophy in soil: a
873 review, Pedosphere 24, 291–307, https://doi.org/10.1016/S1002-0160(14)60016-3, 2014.
874
875 Serreze, M. C., and Barry, R. G.: Processes and impacts of Arctic amplification: A research synthesis, Global Planet. Change,
876 77, 85–96, https://doi.org/10.1016/j.gloplacha.2011.03.004, 2011.
877
878 Sievers, J., Sørensen, L. L., Papakyriakou, T., Else, B., Sejr, M. K., Haubjerg Søgaard, D., Barber, D., and Rysgaard, S.: Winter
879 observations of CO_2 exchange between sea ice and the atmosphere in a coastal fjord environment, Cryosphere, 9, 1701–1713,
880 https://doi.org/:10.5194/tc-9-1701-2015, 2015.
881
882 Stjern, C. W., Lund, M. T., Samset, B. H., Myhre, G., Forster, P. M., Andrews, T., et al.: Arctic amplification response to
883 individual climate drivers, J. Geophys. Res.-Atmos., 124, 6698–6717, https://doi.org/10.1029/2018JD029726, 2019.
884
885 Stull, R. B.: An introduction to boundary layer meteorology, Kluwer Academic Publishers, Dordrecht, ISBN 978-90-277-
886 2769-5, 1998.
887
888 Tan, Z., Zhuang, Q., Henze, D. K., Frankenberg, C., Dlugokencky, E., Sweeney, C., Turner, A. J., Sasakawa, M., and Machida,
889 T.: Inverse modeling of pan-Arctic methane emissions at high spatial resolution: what can we learn from assimilating satellite
890 retrievals and using different process-based wetland and lake biogeochemical models?, Atmos. Chem. Phys., 16, 12649–
891 12666, https://doi.org/10.5194/acp-16-12649-2016, 2016.
892
893 Taylor, M. A., Celis, G., Ledman, J. D., Bracho, R., and Schuur, E. A. G.: Methane efflux measured by eddy covariance in
894 Alaskan upland tundra undergoing permafrost degradation, J. Geophys. Res.-Biogeo., 123(9), 2695–2710,
895 https://doi.org/10.1029/2018J G004444, 2018.
896

Treat, C. C., Virkkala, A.-M., Burke, E., Bruhwiler, L., Chatterjee, A., Fisher, J. B., et al.: Permafrost carbon: Progress on understanding stocks and fluxes across northern terrestrial ecosystems, J. Geophys. Res.-Biogeo., 129, e2023JG007638, https://doi.org/10.1029/2023JG007638, 2024.

Treat, C.C, Bloom, A.A, Marushchak, M.E.: Nongrowing season methane emissions—a significant component of annual emissions across northern ecosystems. Glob. Change Biol.,24:3331–3343, https://doi.org/10.1111/gcb.14137, 2018

Treat, C.C., Natali, S.M., Ernakovich, J., Iversen, C.M., Lupascu, M., McGuire, A.D., Norby, R.J, Chowdhury, T.R., Richter, A., Ruckov, H.S., Schade, C., Schuur, E.A.G., Sloan, V.L., Turetsky, M.R., and Waldrop, M.P.: A pan-Arctic synthesis of CH_4 and CO_2 production from anoxic soil incubations. Glob. Change Biol., 21, 2787–2803, https://doi: 10.1111/gcb.12875, 2015

Uchida, M., Kishimoto, A., Muraoka, H., Nakatsubo, T., Kanda, H., and Koizumi, H.: Seasonal shift in factors controlling net ecosystem production in a high Arctic terrestrial ecosystem, J. Plant Res., 123, 79–85, 2009.

Ueyama, M., Iwata, H., Harazono, Y., Euskirchen, E. S., Oechel, W. C., & Zona, D. (2014). *Growing season and spatial variations of carbon fluxes of Arctic and boreal ecosystems in Alaska (USA). Ecological Applications*, 24(8), 1798–1816. doi:10.1890/13-0725.1

Vaughn, L. J. S., Conrad, M. E., Bill, M., and Torn, M. S. (2016). Isotopic Insights into Methane Production, Oxidation, and Emissions in Arctic Polygon Tundra. Glob. Change Biol. 22 (10), 3487–3502. doi:10.1111/gcb.13281

Vickers, D., and Mahrt, L.: Quality control and flux sampling problems for tower and aircraft data, J. Atmos. Ocean. Tech., 14(3), 512–526, https://doi.org/10.1175/1520-0426(1997)014, 1997.

Voigt, C., Virkkala, A.-M., Gosselin, J. H., Bennett, K. A., Black, T. A., Detto, M., Chevrier-Dion, C., Guggenberger, G., Hashmi, W., Kohl, L., Kou, D., Marquis, C., Marsh, P., Marushchak, M. E., Nesic, Z., Nykänen, H., Saarela, T., Sauheitl, L., Walker, B., Weiss, N., Wilcox, E. J., and Sonnentag, O.: Arctic soil methane sink increases with drier conditions and higher ecosystem respiration, Nature Clim. Change, 13, 1095–1104, https://doi.org/10.1038/s41558-023-01785-3, 2023.

Wagner, I., Hung, J. K. Y., Neil, A., and Scott, N. A.: Net greenhouse gas fluxes from three High Arctic plant communities along a moisture gradient, Arct. Sci., 5, 185–201, https://doi.org/10.1139/as-2018-0018, 2019.

Wang, L., Lee, X., Wang, W., Wang, X., Wei, Z., W., C., Fu, C., Gao., Y., Lu, L., Song, W., Su, P. and Lin, G.: 2017. A Meta-Analysis of open-path eddy covariance observations of apparent CO_2 flux in cold conditions in FLUXNET. J. Atmos. Oceanic Technol., 34, 2475–2487, https://doi.org/10.1175/JTECH-D-17-0085.1, 2017

Wang, Y., Yuan, F., Arndt, K.A., Liu, J., He, L., Zuo, Y., Zona, D., Lipson, D.A., Oechel, W.C., Ricciuto, D.M., Wullschleger, S.D., Thornton, P.E. and Xu, X.: Upscaling Methane Flux From Plot Level to Eddy Covariance Tower Domains in Five Alaskan Tundra Ecosystems. Front. Environ. Sci. 10:939238, doi: 10.3389/fenvs.2022.939238, 2022.

Webb, E. K., Pearman, G. I., and Leuning, R.: Correction of the flux measurements for density effects due to heat and water vapour transfer, Q. J. Roy. Meteor. Soc., 106, 85–100, https://doi.org/10.1002/qj.49710644707, 1980.

Wilczak, J. M., Oncley, S. P., and Stage, S. A.: Sonic anemometer tilt correction algorithms, Bound-Lay. Meteorol., 99, 127–150, https://doi.org/10.1023/A:1018966204465, 2001.

Winther, J.-G., Bruland, O., Sand, K., Gerland, S., Marechal, D., Ivanov, B., Glowacki, P., and König, M.: Snow research in Svalbard - an overview, Polar Research, 22, 125–144, https://doi.org/10.1111/j.1751-8369.2003.tb00103.x, 2003.

947
948 Zona, D., Lafleur, P. M., Hufkens, K., Gioli, B., Bailey, B., Burba, G., Euskirchen, E. S., Watts, J. D., Arndt, K. A., Farina,
949 M., Kimball, J. S., Heimann, M., Göckede, M., Pallandt, M., Christensen, T. R., Mastepanov, M., López-Blanco, E., Dolman,
950 A. J., Commane, R. … Oechel, W. C.: Pan-Arctic soil moisture control on tundra carbon sequestration and plant productivity,
951 Global Change Biol., 29, 1267–1281, https//doi.org/10.1111/gcb.16487, 2022.
952
953 Zona, D., Gioli, B., Commane, R., Lindaas, J., Wofsy, S. C., Miller, C. E., Dinardo, S. J., Dengel, S., Sweeney, C., Karion,
954 A., Chang, R.-W., Henderson, J. M., Murphy, P. C., Goodrich, J. P., Moreaux, V., Liljedahl, A., Watts, J. D., Kimball, J. S.,
955 Lipson, D. A., and Oechel, W. C.: Cold season emissions dominate the Arctic tundra methane budget, P. Natl. Acad. Sci. USA,
956 113(1), 40–45, https://doi.org/10.1073/pnas.15160 17113, 2016.